Cannabinoids shift the basal ganglia microRNA m^{6}A methylation profile towards an anti-inflammatory phenotype in SIV-infected rhesus macaques

Chioma M. Okeoma[1,2*], Lakmini S. Premadasa[3], Chen S. Tan[4], Ionita C. Ghiran[5*], Mahesh Mohan[3*]

[1]Department of Pathology, Microbiology & Immunology, New York Medical College, Valhalla, NY, USA

[2]Lovelace Biomedical Institute, Albuquerque, NM 87108-5127, USA.

[3]Southwest National Primate Research Center, Texas Biomedical Research Institute, San Antonio, TX 78227-5302, USA.

[4]Division of Infectious Diseases, Department of Internal Medicine, University of Iowa, Iowa City, IA 52242, USA

[5] Department of Anesthesia, Critical Care and Pain Medicine, Beth Israel Deaconess Medical Center, Harvard Medical School, Boston, MA, USA

*Correspondence: cokeoma@nymc.edu; ighiran@bidmc.harvard.edu, MMohan@txbiomed.org

Abstract

Background

Epitranscriptomic modifications modulate diverse biological processes like regulation of gene expression, abundance, location and function. N6-methyladenosine (m^6A) methylation has been shown to regulate various diseases, including cancer and inflammation. While there is evidence that m^6A modification is functionally relevant in neural development and differentiation, the role of m^6A modification in HIV neuropathogenesis is unknown.

Methods

Here, we used anti-N6-methyladenosine (m^6A) antibody immunoprecipitation and microarray profiling to identify m^6A modifications in miRNAs in basal ganglia (BG) of Rhesus macaques (RMs) that were uninfected (VEH) and SIV-infected on combination anti-retroviral therapy (cART) and either VEH-treated (VEH/SIV/cART), or THC:CBD-treated (THC:CBD/SIV/cART). Ingenuity pathway analysis was conducted to understand the biological implications of miRNA m^6A methylation in HIV neuropathogenesis. Finally, to understand the functional significance of m^6A modifications in miRNAs, we overexpressed FAM-labeled wild-type or m^6A-modified miR-194-5p in SCC-25 cells and determined its impact on the expression of its target, STAT1, an interferon-stimulated transcription factor known to drive persistent neuroinflammation in several neurodegenerative diseases.

Results

HIV/SIV infection promoted an overall hypomethylated miRNA m^6A profile. While the overall hypomethylated m^6A profile was not significantly impacted by THC:CBD, specific miRNAs predicted to target proinflammatory genes showed markedly reduced m^6A methylation levels

compared to the VEH-treated RMs. Additionally, specific BG tissue miRNAs bearing m^6A epi-transcriptomic marks were transferred and detected in BG-derived extracellular vesicles. Mechanistically, the DRACH motif in the seed region of miR-194-5p was significantly m^6A hypomethylated in THC:CBD/SIV/cART RMs. In SCC-25 cells, unlike wild-type miR-194-5p, transfected m^6A-modified miR-194-5p mimics failed to downregulate STAT1 protein expression. Further, compared to VEH/SIV/cART RMs, THC:CBD administration significantly reduced m^6A methylation of 44 miRNAs directly involved in regulating CNS network genes.

Conclusions

These results underscore the need for investigating the qualitative, and posttranscriptional modifications in RNA along with the more traditional, quantitative alterations in pathological conditions or in response to disease modifying treatments. Our findings indicate that m^6A epitranscriptomic marks in the seed nucleotide region can impair miRNA function and that cannabinoids may preserve it by reducing m^6A methylation levels. Finally, these findings provide a novel mechanistic (miRNA m^6A hypomethylation) explanation underlying the anti-neuroinflammatory effects of phytocannabinoids in HIV/SIV infection.

Keywords

N6-methyladenosine (m^6A), epitranscriptomic marks, post-transcriptional microRNA modification, HIV, SIV, rhesus macaque, cannabinoids, THC, CBD, miR-194-5p, STAT1, neuroinflammation network genes.

Introduction

Despite successful control of HIV with combined antiretroviral therapy (cART)[1-3], up to 50% of persons living with HIV (PLWH) still suffer from HIV Associated Neurocognitive Disorders (HAND)[4, 5]. A major factor driving HAND is incomplete viral suppression in the CNS, and the consequent activation of resident microglia, leading to neuroinflammation and neuronal damage.

In addition, drug abuse is a major comorbidity, where ~40% of PLWH use cocaine and cannabis[6-9], resulting in increased virus-induced pathology[10-15], though cannabis use could afford varying degrees of protection from immune activation/inflammation [7]. While collecting longitudinal blood and matched brain samples from PLWH and healthy controls is extremely challenging, the availability of the SIV-infected RM model supports investigation of phytocannabinoids and other drugs of abuse on HIV/SIV neurological disease progression and has the potential to shed light on the underlying molecular mechanisms. Our previous studies, using the non-human primate (NHP) model, showed that twice daily administration of low-dose delta-9-tetrahydrocannabinol (THC) to RMs significantly reduced expression of type I-interferon (IFN) induced genes including inflammation associated miRNAs, miR-155 and miR-142-3p, in basal ganglia (BG) of cART naïve SIV-infected RMs[16, 17]. The effect of THC on BG was also present in BG-derived extracellular vesicles (EVs). Transcriptomic analyses of miRNAs associated with EVs isolated from these BG tissues revealed that both SIV infection and THC administration induced distinct but significant changes in BG EV-associated miRNAs, which were predicted to regulate pathways related to inflammation/immune regulation, TLR signaling, neurotrophin TRK receptor signaling, and cell death/response[18]. Long-term administration of low-dose THC to SIV infected RMs led to significant upregulation of 37 miRNAs in BG-EVs. Of these 37 miRNAs, 11 miRNAs were significantly downregulated in EVs from SIV infected control RMs that received vehicle control instead of THC.

Recent studies have identified over 170 RNA modifications, among which, m^6A (N6-methyladenosine) is the most abundant modification in mammalian RNA, occurring in ~50% of the total methylated ribonucleotides[19]. RNA m^6A modifications regulate a wide variety of processes such as metabolism, splicing, translation, and degradation of RNA as well as in disease pathogenesis. m^6A modifications have been described not only in mRNA but also recently in miRNAs, a class of small noncoding regulatory RNAs. miRNAs play key roles in regulating protein translation and has been implicated in various neurological disorders, including cognitive impairment. While others and we have published the role of miRNAs in the regulation of gene expression in the brain, there is a significant knowledge gap regarding the role of post transcriptional changes, in particular, miRNA m^6A modification and its implications in HIV/SIV neuropathogenesis. Accordingly, the present study investigated the relationship between HIV/SIV infection of BG, miRNA m^6A alterations, and the potential impact of concurrent phytocannabinoid use on miRNA m^6A modifications and its potential implications for HAND pathogenesis.

Here, we present data supporting shifts in the small RNA landscape in the BG in response to HIV/SIV infection and cART treatment and the impact of concurrent THC:CBD administration. In addition to changes in the expression levels of several miRNA species involved in cognition and neuroinflammation, we also detected for the first-time significant alterations in the m^6A methylation levels of key miRNA species, suggesting an added, more refined level of protein expression control. By exploring the interplay involving HIV/SIV infection, miRNA m^6A alterations in BG, and phytocannabinoid use, this study aims to offer a comprehensive understanding of the role of m^6A modifications on miRNA function that may provide valuable mechanistic insights into the development of HAND and pave the way for novel therapeutic strategies to mitigate cognitive decline in PLWH.

Methods

Animal care, ethics, and experimental procedures

All experiments using RM (**Table 1**) were approved by the Texas Biomedical Research Institute's (Texas Biomed) Institutional Animal Care and Use Committee (Protocols 1734MM). The Southwest National Primate Research Center (SNPRC) is an association for Assessment and Accreditation of Laboratory Animal Care International-accredited facility (AAALAC #000246). The NIH Office of Laboratory Animal Welfare assurance number for the SNPRC is D16-00048. All clinical procedures, including administration of anesthesia and analgesics, were carried out under the direction of a laboratory animal veterinarian. Animals were pre-anesthetized with ketamine hydrochloride, acepromazine, and glycopyrrolate, intubated and maintained on a mixture of isoflurane and oxygen. All possible measures were taken to minimize the discomfort of all the animals used in this study. Texas Biomed complies with NIH policy on animal welfare, the Animal Welfare Act, and all other applicable federal, state and local laws.

Animal model and experimental design

Twelve age and weight-matched male Indian RMs were randomly distributed into three groups (**Table 1**). Group 1 [uninfected controls (n = 4)] served as uninfected controls. Groups 2-3 (n = 38) were infected intravenously with 100 times the 50% tissue culture infective dose (100TCID$_{50}$) of SIVmac251. Group 2 [VEH/SIV/cART] (n = 4) received twice daily injections of vehicle (VEH) (1:1:18 of emulphor:ethanol:saline), intramuscularly. Group 3

[THC:CBD/SIV/cART] (n = 4) received twice daily injection of THC:CBD (1:3 ratio) intramuscularly beginning four weeks after SIV infection at 0.18mg/kg, as used in previous studies[17]. This dose of THC was increased to 0.32mg/kg over a period of 2 weeks and maintained for the duration of the study. For animals in groups 2 and 3 (n = 8), cART was administered daily by subcutaneous injection and included TDF (5.1 mg/kg) (Gilead), Emtricitabine (30mg/kg) (Gilead) and Dolutegravir (3mg/kg) (ViiV Healthcare) and was initiated four weeks post-SIV infection (same time as initiation of cART or VEH injections). Basal ganglia (BG) tissue (~5cm) was collected at necropsy from all animals. A cube of 1x1x1 cm BG tissue was used for total RNA extraction. For histopathological and immunohistochemical evaluation, BG tissues were fixed in Z-fix, embedded in paraffin, sectioned at 5 µM for further analysis. SIV levels in basal ganglia were quantified using the TaqMan One-Step Real-time RT-qPCR assay that targeted the LTR gene[16]. SIV inoculum, infection duration, BG viral loads, and BG histopathology is provided in **Table 1**.

Methylated RNA immunoprecipitation (MeRip).

We have completed the Arraystar Human N6-methyladenosine (m6A) small RNA modification microarray analysis of the samples you submitted. The RNA samples were QC'd for quantity by NanoDrop ND-1000 spectrophotometer and RNA integrity by Bioanalyzer 2100 or gel electrophoresis. Briefly, 1-5 µg of each total RNA sample was immunoprecipitated by 4 µg anti-N6-methyladenosine antibody (Synaptic Systems) with 1 mg Protein G Dynabeads (Thermo Fisher, 11203D) in 500 µL RIP buffer. The modified RNAs were eluted from the immunoprecipitated magnetic beads as the "IP". The unmodified RNAs were recovered from the supernatant as "Sup". The "IP" and "Sup" RNAs were enzymatically labeled with Cy5 and Cy3 respectively in separate reactions using Arraystar's standard protocols. The labeled RNAs were combined and hybridized onto Arraystar Human small RNA Modification Microarray (8x15K,

Arraystar) and the array was scanned in two-color channels by an Agilent Scanner G2505C.Agilent Feature Extraction software (version 11.0.1.1) was used to analyze the acquired array images. Raw intensities of IP (immunoprecipitated, Cy5-labelled) and Sup (supernatant, Cy3-labelled) were normalized with average of log2-scaled Spike-in RNA intensities. After normalization, the probe signals having Present (P) or Marginal (M) QC flags in at least 4 out of 12 samples were retained. Multiple probes from the same small RNA (miRNA/TsRNA (tRF&tiRNA)/pre-miRNA) were combined into one RNA level. “m6A abundance” was analyzed based on the Cy5-labelled IP (modified RNA) normalized intensities. Differentially m6A-modified RNAs between two comparison groups were identified by fold change (FC) and statistical significance (p-value) thresholds. Hierarchical Clustering heatmap was plotted to display m6A-modification patterns among samples by R software.

RNA processing and m^6A analyses

Basal ganglia tissues were collected during necropsy in 1 cm^3 cubes and processed for total RNA extraction using Qiazol (Qiagen Inc, CA). A detailed protocol is provided in the Supplemental methods. Briefly, total RNA was immunoprecipitated with anti-N6-methyladenosine (m6A) antibody and the modified RNAs were eluted from the beads as "m6A," and unmodified RNAs were recovered as "unmodified" samples. Raw intensities of each sample were normalized with average of log2-scaled Spike-in RNA intensities. Differentially m6A-modified RNAs between two comparison groups were identified by fold change (FC) and statistical significance (p-value) thresholds. Hierarchical Clustering heatmap was plotted to display m6A-modification patterns among samples by R software.

Criteria for selecting m^6A modified miRNA

Differentially significant m^6A methylated miRNAs were identified with p-value < 0.05, | log2(FC)| > 1 upregulation, <-1 downregulation). To identify m^6A modified miRNAs that are biologically relevant to HIV/SIV induced neuroinflammation, we used miRNA Target Filter functionality of IPA with a set of criteria to prioritize experimentally validated and predicted mRNA targets to perform enrichment analysis. Based on confidence level, diseases, cells/tissues, and pathways, we identified miRNA-mRNA, overlay miRNA data onto network pathways, and molecules. The identified miRNA target genes were fed into WEB-based GEne SeT AnaLysis Toolkit (WebGestalt, https://www.webgestalt.org/) and used for Geneontology analysis. The following criteria were used:

Tissue = Brain

Pathway = Neurotransmitters and other nervous system signaling

Disease = neurological diseases

Network overlay = neuroinflammation canonical signaling pathway. Merge multiple relevant networks.

Used IPA-generated list for STRING: functional protein association networks (https://string-db.org/) for protein:protein analysis.

Used IPA-generated list for WEB-based Gene SeT AnaLysis Toolkit (WebGestalt) GO biological, cellular, molecular processes analyses, using over representation analysis (ORA) enrichment method.

Cell culture and in vitro transfection studies

We determined the impact of miR-194-5p m6A on STAT1 using human squamous cell carcinoma (SCC-25) epithelial-like cell line (ATCC.org CAT# CRL-1628) as this cell line expressed high basal levels of STAT1 protein. SCC-25 cells were cultured in 1:1 mixture of DMEM and F12 medium (Thermo Fisher scientific, Waltham, MA USA) containing 1.2g/L

sodium bicarbonate, 2.5mM L-glutamine, 15 mM HEPES and 0.5 mM sodium pyruvate and supplemented with 10% FBS in 8 well chamber slides (Cellvis, Mountain view, CA USA) at 37 °C in a humidified atmosphere with 5% CO_2. At 90% confluency, cells were transfected with 30 nM of negative control, miR-194-5p-Wild type or miR-194-5p-m6A mimic using the Lipojet transfection reagent (Signagen, DE). Each treatment was performed in five replicates and repeated twice. At 72 h post-transfection, cells were fixed with 2% paraformaldehyde and immunostained with STAT1 and later with DAPI for nuclear localization.

Immunofluorescence staining, confocal microscopy and data analysis

Immunofluorescence staining for the detection of STAT1 in SCC-25 cells transfected with negative control, miR-194-5p wild type and miR-194-5p m6A modified mimics was performed using STAT1 monoclonal antibody (Cell Signaling technology; Cat# 14994T) (1:200 dilution). A total of 5 images were taken from each well using Zeiss LSM700 confocal microscope (Carl ZEISS Microscopy, LLC) at 20X objective. Digital images were imported into HALO software (Indica Labs) for image quantitation analysis. Area quantification module FL v2.3.4 on HALO v3.6 (Indica Labs) was used to quantify STAT1 fluorescence intensity (red signal/Alexa-568). Artificial intelligence driven HALO software identifies all cells that express STAT1 in red and nuclei in blue (DAPI) and categorizes the cells based on fluorescence intensity levels. The average fluorescence intensity per each transfected well (5 replicates per condition) in 8 well chambers was calculated, and the data were graphed using Prism v9 (GraphPad Prism software).

Statistical analysis

Pie Charts were generated using GraphPad Prism. Heatmaps were generated with GraphPad Prism and Heatmapper (http://heatmapper.ca/). Venn diagrams were generated with Venny 2.1 (https://bioinfogp.cnb.csic.es/tools/venny/). Changes in STAT1 protein expression in response to miR-194-5p transfection was analyzed using One-way ANOVA. Post hoc analysis was performed using Tukey's multiple comparison's test. Shapiro-Wilk test (GraphPad Prism) was used to test for data normality.

Results

Quantification of m^6A profiles of BG miRNAs point to mechanistically relevant species involved in the anti-inflammatory effect of THC:CBD treatment

Altered m6A-modified RNA expression levels in the brain were linked to dysregulation of key genes involved in immune cell activation, cytokine production, and blood-brain barrier integrity, which could modulate the activation of microglia and astrocytes, thereby, initiating and exacerbating neuroinflammatory processes[20, 21]. Most of the published research regarding the role of m6A changes in neuroinflammation has centered on mRNA and lncRNA and not miRNA molecules (reviewed in[22]. Hence, we focused exclusively on miRNAs in the present study.

All seven SIV-infected RMs, receiving either VEH (n=4) or THC:CBD (n=3), had substantial plasma viral loads ranging from 1.93 to 16.8 x 10^6 copies/mL during acute infection [12-20 days post SIV infection (DPI)] (**Table 1**). However, cART initiation at 30 DPI effectively suppressed viral replication, as viral RNA was undetectable in both plasma and BG at necropsy (180 DPI).

We investigated how SIV infection and/or THC:CBD altered the landscape of m^6A changes in miRNAs isolated from BG of RMs that were either i) uninfected (Control), ii) SIV-

infected, treated with cART and administered either vehicle (VEH) alone (VEH/SIV/cART), or iii) SIV-infected, treated with cART and administered THC:CBD (THC-CBD/SIV/cART). The m^6A analyses were performed by microarray hybridization profiling following pull down of m^6A modified miRNAs using an m^6A specific antibody (Synaptic Systems). BG tissues from all three groups were analyzed for miRNA m^6A modifications. After quality control and filtering, we used a p-value (unpaired t-test) <= 1.0 and fold-change >= 0.0 to identify a total of 1805 miRNAs that were m^6A modified in all experimental groups irrespective of statistical significance (**Supplemental Table 1**). We compared each treatment group to the uninfected control group and found that SIV infection induced a significantly broader m^6A hypomethylation of BG miRNAs (**Table 2**) compared to hypermethylation. Of the total 1805 miRNAs in the VEH/SIV/cART group with m^6A modifications, 1281 (71%) were mature miRNAs, while 524 (29%) were passenger strand (PS) miRNAs (generated from the opposite (3') strand) (**Fig. 1A**). Over 95% of the mature and PS miRNAs were m^6A hypomethylated in VEH/SIV/cART (**Fig. 1B**) and in THC:CBD/SIV/cART (**Fig. 1C**) RMs compared to uninfected controls (**Figs. 1B, 1C**). In contrast, only 6% and 5% of mature and PS miRNAs, respectively, were hypomethylated when comparing VEH/SIV/cART to THC:CBD/SIV/cART (**Fig. 1D**) RMs. Raw intensities of IP of m^6A- and unmodified-miRNA species, respectively, were normalized with average of log2-scaled spike-in RNA intensities. We found an overall inverse relationship between m^6A methylation and expression abundance of the miRNA species in VEH/SIV/cART (**Fig. 1E**) and THC:CBD/SIV/cART (**Fig. 1F**) RMs when compared to controls, and that of VEH/SIV/cART when compared to THC:CBD/SIV/cART (**Fig. 1G**) RMs. Our data presented above show that while unsupervised clustering of the differentially expressed miRNAs species isolated from BG fails to separate the control from the THC:CBD treated group, analyses of the differentially m^6A-modified miRNA clearly identifies changes in the miRNA profile promoted by the THC:CBD treatments, underscoring the need for functional quantification of the RNA levels in addition to the canonical up and down quantifications.

SIV infection increased the overall m^{6}A methylation levels in BG-derived miRNAs

Further analyses of the m^{6}A methylated miRNAs were conducted to identify significantly m^{6}A modified miRNAs using p-value < 0.05 (unpaired t-test) and fold change >= 1.5. We found that most of the m^{6}A modified miRNAs were present in mature miRNAs with percentages ranging from 60 to 72% (**Figs. 2A-F**). While SIV infection induced significant hypo m^{6}A modifications in BG miRNAs in over 1000 miRNA species when compared to control animals, hypermethylation changes were identified in only seven miRNA species (**Table 3**). We next compared methylation levels with miRNA abundance (expression), by calculating the miRNA abundance using mean m^{6}A RNA modification quantity per treatment, mean m^{6}A RNA modification quantity for control, and the difference of mean percentage of m^{6}A RNA modification (%Modified) between the treatment and control groups. The levels of the m^{6}A modification versus abundance are displayed as heatmaps (**Figs. 2G-L**). The top 5 miRNAs or fewer (depending on the group) were selected and their m^{6}A and expression levels are presented as heatmaps (**Figs. 2M-R**).

Pathway analysis of SIV-induced m^{6}A epitranscriptomic marks in BG miRNAs of SIV-infected RMs identified top neuroinflammation network genes

To analyze the biological implications of m^{6}A-enriched miRNAs, we used ingenuity pathway analysis (IPA) to perform enrichment analysis of predicted and validated genes targeted by hypo or hyper m^{6}A methylated miRNAs (**Supplemental Table 1**) using criteria determined apriori. We identified neuroinflammation network genes associated with the miRNAs from each group that were hypomethylated (**Supplemental Fig. 1 left, Fig. 3A**) or hypermethylated (**Supplemental Fig. 1 right, Fig. 3B**). The top 35 IPA neuroinflammation network genes associated with m^{6}A hypo and hyper methylated miRNAs are shown in **Table 4**. In addition to

the protein networks altered by the m^6A methylated miRNAs, our results also identified several miRNA species which were also targeted by the m^6A-modified miRNAs. These data are consistent with previous reports that demonstrated regulation of primary miR-21 by mature miR-122 [23-25].

Integration of IPA and GO analyses.

Our analyses identified several disease-related functional clusters linked to neuroinflammation network genes associated with m^6A hypo and hyper methylated miRNAs (**Table 5**). Whereas the top three diseases related to changes in invasion, migration, and proliferation of cells, were linked to a hypomethylated m^6A profile (rows 1-4), diseases associated with changes in quantity of cells, organization of cytoskeleton, and neurotransmission were linked to the hypermethylated m^6A profile (rows 1-3). Integration of IPA and the 35 neuroinflammation genes with WEB-based Gene SeT Analysis Toolkit (WebGestalt) GO analysis identified several biological processes, cellular components, and molecular functions of the neuroinflammation network genes for each group that stratified into targets of hypomethylated m^6A (**Fig. 4A**) and hypermethylated m^6A (**Fig. 4B**).

Conjoint Analysis of m^6A methylation and differentially altered miRNA expression

We next determined the functional significance of m^6A methylation of miRNAs, by first determining the relative abundance of the m^6A hypo and hyper methylated miRNAs species. After obtaining the abundance of miRNAs with significant m^6A modifications, we found that majority of significantly m^6A-modified miRNAs were either significantly up or down regulated (**Table 6**). We also found a positive correlation between m^6A methylation and miRNA abundance for Hypo_VEH/SIV/cART_vs_Controls (Pearson $r=0.72$; $p<1e-10$) and

Hypo_THC:CBD/SIV/cART_vs_Controls (Pearson r=0.84; $p<1e^{-10}$) (**Figs. 5A, 5B)**, respectively. However, we did not identify any additional correlations among other treatment groups (**Supplemental Fig. 2**). To examine the functional relationship of m^6A methylated miRNAs, we used IPA miRNA Target Filter focused on miRNAs related to neurotransmitter networks and nervous system-centered signaling pathways (**Figs. 5C-H, Table 7**). Analysis of protein:protein interactions (PPI) for the IPA identified miRNA targets using STRING: functional protein association networks (*https://string-db.org/*) led to the identification of several gene clusters and nodes associated with the m^6A methylation status (hypermethylation vs hypomethylation) and miRNA abundance that may shed light into the potential biological functions of miRNA m^6A methylation (**Figs. 5I-N**). The potential biological functions of the miRNA targets were further revealed by GO biological processes, molecular functions, cellular components, Kegg/Reactome/Wiki pathways, disease gene associations, and tissue expressions (**Table 8**).

THC:CBD administration significantly reduced the m^6A levels in the seed sequence of HIV/SIV-altered miRNAs regulating neuroinflammation

Relative to the THC:CBD/SIV/cART group, 44 miRNAs showed significant m^6A hypermethylation in the VEH/SIV/cART RMs (**Fig. 6A**). More importantly, IPA analyses of the genes targeted by the 44 miRNAs that were hypermethylated in BG of VEH/SIV/cART compared to THC:CBD/SIV/cART RMs (**Table 8**) identified neuroinflammation gene networks previously shown to drive neuroinflammation, neuropathogenesis of Huntington's, Alzheimer's, and Parkinson's disease (**Fig. 6B**). Key biological processes regulated by these m^6A hypermethylated miRNAs included gamma-aminobutyric acid signaling pathway, synaptic transmission, cognition, immune-response regulating signaling pathway and positive regulation of cytokine production (**Fig. 6C**). GABA receptor activity, glutamate receptor activity, neurotransmitter receptor activity, gated channel activity, cytokine receptor activity were the

most significant molecular functions enriched for these mRNA targets. Additionally, the targets of the miRNAs associated with KEGG were linked to GABAergic synapse, leishmaniasis, and nicotine addiction. Reactome pathways are linked to Toll-like receptor 5 cascade, MyD88 cascade, neurotransmitter receptors and postsynaptic signal transmission, signaling by interleukins, and cytokine signaling in the immune system. Diseases associated with autistic disorder, asthma reperfusion injury, atherosclerosis, substance withdrawal syndrome, nerve degeneration, cholestasis, myocardial reperfusion injury, urticaria, hepatic encephalopathy (**Supplemental Figs. 3A-C**). Further analysis of the 44 m^6A hypermethylated miRNA revealed RRACH or DRACH motif in 14 out of the 44 miRNAs (**Table 9**), indicating that the rest of the m^6A methylation events took place in non-canonical DRACH motives[26]. IPA network linked the targets of the 14 miRNAs with RRACH or DRACH motif to canonical signaling pathways of NF-kB activation by viruses, neuroinflammation signaling, and transcriptional activity by SMAD heterotrimer, all of which are functionally linked to cognitive impairment[27-29] (**Fig. 6D**).

M6A marks in the miR-194-5p seed region impaired its post-transcriptional silencing potential of the proinflammatory STAT1 protein in vitro

Since miR-194-5p showed significantly more m^6A hypomethylation in the BG of THC:CBD/SIV/cART (-1.6683 log2 Fold change or -3.178 Fold change) that VE/SIV/cART (-0.8617 log2 Fold change or -1.817 fold change) RMs compared to controls and ~1.74-fold (p=0.06) more hypomethylation in BG of THC:CBD/SIV/cART relative to VEH/SIV/cART RMs (**Fig. 7B** and **Supplemental Table 1**), we hypothesized that this would allow miR-194-5p to more effectively downregulate its highly conserved (**Fig. 7A**) [30] predicted target gene, STAT1, an interferon-gamma stimulated transcription factor known to activate the expression of interferon-stimulated immune response genes and drive neuroinflammation in PWH and SIV infected RMs [31]. To investigate the impact of m^6A epitranscriptomic marks on miR-194-5p-

STAT1 interactions, we synthesized locked nucleic acid conjugated FAM-labeled m^6A methylated miR-194-5p (in the seed nucleotide region) mimics along with wild-type miR-194-5p and negative control (NC) mimics and transfected SCC-25 oral squamous cell carcinoma cells. We used SCC-25 cells since they expressed high basal STAT1 protein levels. In contrast, most of the neuronal cells we considered including neuroblastoma cells showed very low to no basal STAT1 protein expression. The miR-194-5p-STAT1 duplex was found to have a minimum free energy of -19.8 kcal/mol (**Fig. 7C**). As evident in **Fig. 7E1** and **E2**, transfection of SCC-2 cells with 30 nM wild type miR-194-5p significantly reduced STAT1 protein expression compared to the wells transfected with negative control (**Fig. 7D1**, **D2** and **G**). Consistent with our hypothesis, adding m^6A marks to the DRACH motif in the miR-194-5p seed region (**Fig. 7B**) significantly diminished its ability to suppress STAT1 protein expression (**Fig. 7F1**, **F2** and **G**). Accordingly, m6A modified miR-194-5p transfected cells showed significantly higher STAT1 protein expression compared to the cells transfected with wild type miR-194-5p (**Fig. 7F1**, **F2** and **G**) and was similar to the wells transfected with the NC mimic (**Fig. 7D1**, **D2** and **G**).

Basal ganglia tissue miRNAs enriched in m^6A modification are also present in basal ganglia-derived Extracellular Vesicles (EVs)

We integrated BG tissue miRNA abundance with miRNA counts from our previously published BG derived EVs (BG EVs) miRNA sequence dataset [18] to identify tissue miRNAs with m^6A modifications that were also present in the BG EVs dataset. Of the 527 miRNAs identified in EVs from the BG of SIV infected RMs, 162 (11.1%) were also present in RM whole BG tissues (**Fig. 8A**). Although methylation analyses were not conducted on the EV derived miRNAs, all 162 miRNAs were m^6A hypomethylated in the BG tissues and none of the m^6A hypermethylated miRNAs were present in EVs, suggesting either a sorting mechanism based on the methylation status of the miRNAs, or an active de-methylation process performed by m^6A erasers, which

may be present in EVs (**Fig. 8A**). The top 5 EV-associated miRNAs belonged to the let-7 family (let-7a-5p, let-7c-5p, let-7b-5p, miR-26a-5p, let-7f-5p) (**Fig. 8B**) and were different from the top 5 (miR-320b, miR-504-3p, miR-1224-5p, miR-372-3p, miR-193b-5p) miRNAs found in BG tissues (**Fig. 8C**). Next, we used IPA to identify target genes of the 162 BG tissue-EVs miRNAs that were linked to neuroinflammation canonical pathways (**Fig. 8D**). The target genes were used to predict protein-protein interactions to gain insight into potential direct (physical) and indirect (functional) associations. Three gene clusters were identified (**Fig. 8E**). Their predicted GO biological processes detected included processes related to uterine wall breakdown, negative regulation of interleukin-23 production, positive regulation of EMT involved in endocardial cushion formation, positive regulation of tight junction disassembly, positive regulation of additional functions and signaling pathways (**Table 10).** Furthermore, we used WebGestalt to translate the 162 tissue-EV miRNA target gene lists into biological/functional insights using over representation analyses (ORA) with the Benjamini-Hochberg procedure aimed at reducing the false discovery rate and avoiding type I errors. Ten functional categories were enriched, including neuron death, positive regulation of response to external stimulus, leukocyte proliferation, positive regulation of cell motility, regulation of leukocyte, response to molecule of bacterial origin, T cell activation, regulation of cell-cell adhesion, positive regulation of cell activation, extrinsic apoptotic signaling pathway (**Fig. 6F**). The gene list involved in each of the functional categories is presented in **Table 11**.

Discussion

Despite the widespread application of multi-omics (mRNA, microRNA and LncRNA profiling) technologies to understanding the pathogenesis of HAND, the field of “epi-transcriptomics” involving post-transcriptional regulation of gene expression via RNA modifications and editing that impacts RNA folding, stability and interaction with its targets remains an underexplored and

understudied topic in HIV/SIV infection. Except for a few *in vitro* reports, there exists a dearth of knowledge about m^6A modifications, the most researched epitranscriptomic modification of eukaryotic RNAs in host–HIV interactions. Moreover, the presence of m^6A modifications in small RNAs, such as microRNAs (miRNA), and how HIV infection modulates m^6A modifications in miRNAs during infection is unknown and unexplored. We have previously described the role of miRNAs (both tissue and extracellular vesicle derived) in HIV/SIV induced neuroinflammation and its modulation by long-term low-dose phytocannabinoids. Accordingly, to address this knowledge gap, here, we investigated the profile of BG m^6A methylome in host miRNAs during HIV/SIV infection and the potential effects of phytocannabinoids (THC and CBD) on the BG miRNA m^6A methylome. We used a combination of THC and CBD (1:3) because findings from clinical studies have confirmed that THC is well-tolerated when administered in combination with CBD[32-34]. Specifically, CBD diminished the adverse effects of THC, such as tachycardia, intoxication, and sedation, while preserving the beneficial effects of reduced muscle spasticity and neuroinflammation [32-34].

We detected m^6A modifications of miRNAs from BG tissues of all RMs, irrespective of infection or long-term administration of low-dose phytocannabinoids (THC:CBD). Interestingly, miRNAs from BG tissues of VEH/SIV/cART and THC:CBD/SIV/cART RMs bore significant hypomethylated m^6A profile compared to uninfected control (VEH) RMs with predictive link to neuroinflammation network genes. The potential functional impact of m^6A methylation on miRNA function became clearer when we performed a pathway analysis (IPA) of the genes targeted by the 44 miRNAs that were hypermethylated in BG of VEH/SIV/cART compared to THC:CBD/SIV/cART RMs (**Table 2)**. Hypermethylation of miRNA adenine nucleotides in or near the miRNA seed region (nucleotide positions 2 to 7 in the 5' seed region) can lead to loss of target mRNA 3' UTR binding and repression[35]. Therefore, in a neuroinflammatory disease like HIV/SIV infection, miRNA m^6A hypermethylation could lead to enhanced proinflammatory gene expression and disease progression. IPA processing of the target genes identified numerous

neuroinflammatory genes such as STAT1, CCL2, CXCL12, IFNA4, TIRPA, NOS2, IL6R, IL34, all known to promote neuroinflammation and drive progression of numerous neurological diseases such as Huntington's, Alzheimer's, and Parkinson's disease, (**Fig 5**). Interestingly, others[31] and we[17] have also shown significantly increased expression of type-I IFN stimulated genes in the brains of SIV-infected RMs. To the best of our knowledge, we provide the first evidence of the presence of m^6A modifications with a shift towards significant m^6A hypomethylation in mature miRNAs in the brain during HIV/SIV infection.

The presence of m^6A modified mature miRNAs was recently reported in HEK293T[36], human lung cancer cells, and fibroblast cells in response to hypoxia[35, 37]. Here, using the SIV-infected RM model, we profiled and identified differential m^6A methylation in both mature and PS miRNAs in whole BG tissues, although majority of the m^6A modified miRNAs detected originated from the mature strand. While SIV infection triggered a significant hypomethylated profile in BG tissue miRNAs, miRNA expression abundance was inversely correlated to m^6A methylation in VEH/SIV/cART and THC:CBD/SIV/cART RMs compared to controls RMs. We also identified a set of BG tissue miRNAs [(n=162) ~11.1%] with m^6A epitranscriptomic marks that were also present in BG EVs[18] (**Figure 6**). All 162 BG tissue-EV miRNAs that bore m^6A marks were hypomethylated and none were hypermethylated.

Next, we used IPA and WebGestalt to predict the potential functional relevance of m^6A modified miRNAs. Interestingly, miRNAs bearing m^6A marks were found to have a link to neuroinflammation network genes, neurotransmitters/other nervous system, and pathogen influenced signaling pathways. The top three functional classifications included invasion, migration, and proliferation of cells in generalized disease states linked to m^6A hypomethylation profile while quantity of cells, organization of cytoskeleton, neurotransmission were the important functional groups/processes found to be linked to the hypermethylated m^6A profile (**Table 4**). PPI predicted functions and signaling pathways of BG tissue m^6A-enriched miRNAs that were also present in BG EVs, revealed GO biological processes that included negative

regulation of interleukin-23 production, positive regulation of EMT involved in endocardial cushion formation, positive regulation of tight junction disassembly, and positive regulation of calcidiol 1-monooxygenase activity (**Table 8**), all with potential relevance to HIV/SIV induced neurological disease. Recent studies have shown that m^6A hypermethylation in the seed regions of mature miRNAs resulted in loss of target mRNA recognition, binding, and translational inhibition[35]. Accordingly, based on these predicted functions, it is plausible that the generalized m^6A hypomethylation may be a host response to enable m^6A hypomethylated miRNAs to successfully regulate the expression of proinflammatory mediators, such as IL-23, STAT1, NOS1, and the blood brain barrier integrity by promoting posttranscriptional gene silencing.

Although SIV infection decreased m^6A modifications of BG tissue miRNAs, Lichinchi et al., found that in T cells, HIV infection increased m^6A marks in both host and viral mRNAs [38]. Altogether, our findings show that BG miRNA m^6A modifications may play important roles in host–HIV interactions, as previously suggested in other viral infections, although those studies focused entirely on mRNAs [38-40] and not miRNAs.

From a functional perspective, m^6A miRNA modifications in BG tissues may represent a potential mechanism to regulate host miRNA dependent regulation of proinflammatory gene expression that can directly impact HIV neuropathogenesis. This is evident from recent studies showing m^6A methylation of the adenine residue/s in miR-21-5p[35], where m^6A modification of adenine residues near but not in the seed region resulted in loss of target gene (MAPK10 and PTEN) repression in A549 cells. Therefore, the significantly reduced m^6A methylation in 44 neuroinflammatory gene targeting miRNAs in the THC:CBD/SIV/cART compared to the VEH/SIV/cART group suggests that cannabinoids may preserve the post-transcriptional gene regulatory functions of anti-inflammatory miRNAs by reducing their m^6A epitranscriptomic marks. Our recently published studies found long-term low-dose THC administration to significantly reduce type I-interferon stimulated gene expression[17]. Since type-I IFNs activate

STAT1[41], we performed bioinformatics analysis using TargetScan 8.0 and identified RM STAT1 to be a predicted target of miR-194-5p with a perfect match between the seed sequence of miR-194-5p and the 3' UTR region of STAT1 (**Fig. 7A**). Interestingly, miR-194-5p showed markedly more hypomethylation in THC:CBD/SIV/cART (-1.6683 log2 Fold change) than VEH/SIV/cART (-0.8617 log2 Fold change) compared to control RMs. Increased STAT1 activated by interferons (IFN) is known to drive persistent neuroinflammatory signaling in a variety of neurological diseases such as Alzheimer's, Parkinson's, Huntington's disease and traumatic brain injury. In addition, significant upregulation of IFN-stimulated STAT1 protein expression in the brain has been confirmed by others in the SIV-infected RM model[31]. We further identified a DRACH motif (where, D= A, G or U; U, R= A or G, and H=A, C or U) in the seed region (nucleotides 2-7 from the 5' end) of miR-194-5p (5'-UG**UAA*CA**GC**AACU**CCAUGUGGA-3').

Under in vitro conditions, m^6A methylation of adenine residues in mature miRNAs resulted in reduced suppression of target gene expression[35], suggesting that m^6A modification of miRNA seed nucleotides can interfere with mRNA target recognition and binding. Consistent with the findings of Wang et al. [35], in vitro overexpression of miR-194-5p mimics containing m^6A methylated adenosine nucleotides in the seed region failed to downregulate STAT1 protein expression, while wildtype miR-194-5p significantly reduced STAT1 protein expression at 72 h post transfection. Overall, these findings suggest that the presence of m^6A marks in the miR-194-5p seed region could potentially destabilize A:U pairing, thereby weakening its interactions with its binding region in the 3' UTR of STAT1 mRNA. On the contrary, reduced m^6A methylation of miR-194-5p can preserve its target binding capacity and represents a potential posttranscriptional gene silencing mechanism by which THC or THC:CBD may reduce STAT1 expression and accordingly reduce proinflammatory signaling in the brain and periphery. It is possible that THC:CBD may mediate these changes through altering the expression levels of m^6A writers and erasers that catalyze the addition and removal of m^6A epitranscriptomic marks.

While we m^6A marks in the miR-194-5p seed region interfered with its ability to downregulate STAT1 protein expression, it remains to be determined how m^6A marks in the 3' and regions adjacent to seed nucleotide impact miRNA function. Therefore, future studies are needed to address these knowledge gaps including whether extracellular miRNAs bear similar m^6A marks and the implications of such epitranscriptomic marks in HIV neuropathogenesis.

Declarations:

Consent for publication: All authors read and approved the publication of this manuscript.

Competing interests: The authors report no biomedical financial interests or potential conflicts of interest.

Availability of data and materials: The dataset is included within the article and its additional files.

Funding: This work was supported by National Institutes of Health funding (Grant No. R01DA042348 [to CMO]; Grant Nos. R01DA042524 and R01 DA052845 [MM], Grant Nos. R01DA050169 and R21/R33DA053643 [to CMO & MM], R01CA218500, UH3TR002881, R01TR218500 [to IG], P30AI161943, and P51OD111033.

Author contributions: Study conceptualization and design: IG, CST and MM. CMO conducted data analyses. CMO, MM, and IG wrote the original draft, reviewed and edited the manuscript. IG, LSP and MM performed the in vitro m^6A miR-194-5p overexpression and immunofluorescence studies and HALO image analysis and quantification. LSP assisted with the viral load quantification, manuscript proof reading and preparation of animal information.

Figure legends

Figure 1: Global m^6A methylation patterns basal ganglia miRNAs of RM infected with SIV and treated with THC, cART, or both THC and cART over uninfected controls: A) Percent mature and star miRNAs with m^6A methylation marks. B-D) m^6A methylation patterns in each treatment group. E-G) Heatmap of m6A methylation profile versus miRNA abundance.

Figure 2: The m6A Content of RM basal ganglia tissues was changed by SIV and THC:CBD: A-F) Pie chart representing % of mature and star miRNAs with m^6A modifications. G-L) Heatmap illustrating the levels of the m^6A methylated miRNAs and their abundance. M-R) Heatmap of Top 5 miRNAs from panels G-L.

Figure 3: IPA Pathway analysis of m^6A methylation of basal ganglia miRNAs: A) Neuroinflammation network molecules associated with the with miRNAs with m^6A hypomethylation (left) or hypermethylation (right). B) Two-way Venny of top 35 network molecules between the hypomethylated and hypermethylated miRNA within each animal

groups. C) Three-way Venny of top 30 network molecules comparing m^6A hypomethylated versus hypermethylated miRNA irrespective of animal groups.

Figure 4: Gene ontology (GO) analysis illustrating biological processes, cellular components, and molecular functions of the neuroinflammation network molecules for each animal with m^6A: A) hypomethylated and B) hyper methylated miRNA.

Figure 5: Basal ganglia miRNA with significant m^6A modifications have altered expression levels. A) Correlation analysis of m^6A methylation versus miRNA abundance. C-H) Functional relationship of m^6A methylated miRNA with neurotransmitters/other nervous system and pathogen influenced signaling pathways. I-N) PPI networks for the IPA identified miRNA targets in panels C-H.

Figure 6: THC:CBD administration significantly reduced the incorporation of m^6A epitranscriptomic marks on neuroinflammation targeting miRNAs that were increased by HIV/SIV infection: A) Heatmap of 44 miRNAs with significant m^6A hypermethylation in the VEH/SIV/cART RMs relative to THC:CBD/SIV/cART group. **B**) IPA network interactome and associated canonical signaling pathways and biological functions. **C**) Key biological processes, cellular components, and molecular functions regulated by 44 m^6A hypermethylated miRNAs. **D**) IPA network of canonical signaling pathways and functions associated with 14 miRNAs with RRACH or DRACH motif.

Figure 7: m^6A marks in the seed region of miR-194-5p impairs its ability to post-transcriptionally silence STAT1 expression. A) Conservation of miR-194-5p binding site in the 3' UTR of STAT1 across twelve different mammalian species identified using TargetScan 8.0. **B)** miR-194-5p fold change in VEH/SIV/cART and THC:CBD/SIV/cART relative to control

rhesus macaques. **C)** miR-194-5p-STAT1 pairing as revealed by RNAhybrid has a mean free energy change of -19.8 Kcal/mole. STAT1 protein expression (red) in SCC-25 cells at 72 h post transfection with 30 nM FAM-labeled negative control mimic (**D1** and **D2**), and wild-type (**E1** and **E2**) or m^6A modified (**F1** and **F2**) (green) miR-194-5p mimics and its quantification using HALO AI software (**G**). Transfections were performed in five triplicate wells for each mimic and experiments were repeated twice. Data were analyzed using One-way ANOVA and post hoc analysis was done using Tukey's multiple comparison's test. $P<0.05$ was considered statistically significant.

Figure 8: Identification of tissue-EV miRNA with m6A modification: A) 3-way Venn diagram identifying m^6A modified tissue miRNA present in EVs. B) Top 5 miRNAs in EVs. C) Top 5 miRNAs in tissues. C) Functional relationship of EV-Tissue miRNA with neurotransmitters/other nervous system and pathogen influenced signaling pathways. E) PPI networks for the IPA identified EV-Tissue miRNA targets in panels D. F) Volcano plot of biological/functional insights for EV-Tissue miRNA target gene sets.

Supplemental Figure 1: IPA Pathway analysis of m^6A methylation of basal ganglia miRNAs: A) Neuroinflammation network molecules associated with the with miRNAs with m6A hypomethylation (left) or hypermethylation (right).

Supplemental Figure 2: Correlation analysis of m^6A methylation versus miRNA abundance:

Supplemental Figure 3: Web Gestalt analysis for A) KEGG, **B)** Reactome, **C)** Diseases.

References

1. Eden A, Fuchs D, Hagberg L, Nilsson S, Spudich S, Svennerholm B, Price RW, Gisslen M: **HIV-1 viral escape in cerebrospinal fluid of subjects on suppressive antiretroviral treatment.** *The Journal of infectious diseases* 2010, **202:**1819-1825.
2. Lamers SL, Gray RR, Salemi M, Huysentruyt LC, McGrath MS: **HIV-1 phylogenetic analysis shows HIV-1 transits through the meninges to brain and peripheral tissues.** *Infection, genetics and evolution : journal of molecular epidemiology and evolutionary genetics in infectious diseases* 2011, **11:**31-37.
3. Spudich S, Lollo N, Liegler T, Deeks SG, Price RW: **Treatment benefit on cerebrospinal fluid HIV-1 levels in the setting of systemic virological suppression and failure.** *The Journal of infectious diseases* 2006, **194:**1686-1696.
4. Grant I, Atkinson JH, Hesselink JR, Kennedy CJ, Richman DD, Spector SA, McCutchan JA: **Evidence for early central nervous system involvement in the acquired immunodeficiency syndrome (AIDS) and other human immunodeficiency virus (HIV) infections. Studies with neuropsychologic testing and magnetic resonance imaging.** *Annals of internal medicine* 1987, **107:**828-836.

5. Sacktor N, Skolasky RL, Seaberg E, Munro C, Becker JT, Martin E, Ragin A, Levine A, Miller E: **Prevalence of HIV-associated neurocognitive disorders in the Multicenter AIDS Cohort Study.** *Neurology* 2016, **86:**334-340.

6. Fuster-RuizdeApodaca MJ, Castro-Granell V, Garin N, Laguía A, Jaén Á, Iniesta C, Cenoz S, Galindo MJ: **Prevalence and patterns of illicit drug use in people living with HIV in Spain: A cross-sectional study.** *PLoS One* 2019, **14:**e0211252.

7. Castro FOF, Silva JM, Dorneles GP, Barros JBS, Ribeiro CB, Noronha I, Barbosa GR, Souza LCS, Guilarde AO, Pereira A, et al: **Distinct inflammatory profiles in HIV-infected individuals under antiretroviral therapy using cannabis, cocaine or cannabis plus cocaine.** *Aids* 2019, **33:**1831-1842.

8. Galaj E, Bi GH, Yang HJ, Xi ZX: **Cannabidiol attenuates the rewarding effects of cocaine in rats by CB2, 5-HT(1A) and TRPV1 receptor mechanisms.** *Neuropharmacology* 2020, **167:**107740.

9. Mimiaga MJ, Reisner SL, Grasso C, Crane HM, Safren SA, Kitahata MM, Schumacher JE, Mathews WC, Mayer KH: **Substance use among HIV-infected patients engaged in primary care in the United States: findings from the Centers for AIDS Research Network of Integrated Clinical Systems cohort.** *Am J Public Health* 2013, **103:**1457-1467.

10. Mohammadi A, Darabi M, Nasry M, Saabet-Jahromi MJ, Malek-Pour-Afshar R, Sheibani H: **Effect of opium addiction on lipid profile and atherosclerosis formation in hypercholesterolemic rabbits.** *Exp Toxicol Pathol* 2009, **61:**145-149.

11. Roohafza H, Talaei M, Sadeghi M, Haghani P, Shokouh P, Sarrafzadegan N: **Opium decreases the age at myocardial infarction and sudden cardiac death: a long- and short-term outcome evaluation.** *Arch Iran Med* 2013, **16:**154-160.

12. Nabati S, Asadikaram G, Arababadi MK, Shahabinejad G, Rezaeian M, Mahmoodi M, Kennedy D: **The plasma levels of the cytokines in opium-addicts and the effects of**

opium on the cytokines secretion by their lymphocytes. *Immunol Lett* 2013, **152:**42-46.

13. Saha B, Momen-Heravi F, Kodys K, Szabo G: **MicroRNA Cargo of Extracellular Vesicles from Alcohol-exposed Monocytes Signals Naive Monocytes to Differentiate into M2 Macrophages.** *J Biol Chem* 2016, **291:**149-159.

14. Momen-Heravi F, Saha B, Kodys K, Catalano D, Satishchandran A, Szabo G: **Increased number of circulating exosomes and their microRNA cargos are potential novel biomarkers in alcoholic hepatitis.** *J Transl Med* 2015, **13:**261.

15. Momen-Heravi F, Bala S, Kodys K, Szabo G: **Exosomes derived from alcohol-treated hepatocytes horizontally transfer liver specific miRNA-122 and sensitize monocytes to LPS.** *Sci Rep* 2015, **5:**9991.

16. McDew-White M, Lee E, Alvarez X, Sestak K, Ling BJ, Byrareddy SN, Okeoma CM, Mohan M: **Cannabinoid control of gingival immune activation in chronically SIV-infected rhesus macaques involves modulation of the indoleamine-2,3-dioxygenase-1 pathway and salivary microbiome.** *EBioMedicine* 2022, **75:**103769.

17. McDew-White M, Lee E, Premadasa LS, Alvarez X, Okeoma CM, Mohan M: **Cannabinoids modulate the microbiota-gut-brain axis in HIV/SIV infection by reducing neuroinflammation and dysbiosis while concurrently elevating endocannabinoid and indole-3-propionate levels.** *J Neuroinflammation* 2023, **20:**62.

18. Kaddour H, McDew-White M, Madeira MM, Tranquille MA, Tsirka SE, Mohan M, Okeoma CM: **Chronic delta-9-tetrahydrocannabinol (THC) treatment counteracts SIV-induced modulation of proinflammatory microRNA cargo in basal ganglia-derived extracellular vesicles.** *J Neuroinflammation* 2022, **19:**225.

19. Jonkhout N, Tran J, Smith MA, Schonrock N, Mattick JS, Novoa EM: **The RNA modification landscape in human disease.** *Rna* 2017, **23:**1754-1769.

20. Fan Y, Lv X, Chen Z, Peng Y, Zhang M: **m6A methylation: Critical roles in aging and neurological diseases.** *Front Mol Neurosci* 2023, **16:**1102147.

21. Zhang F, Ran Y, Tahir M, Li Z, Wang J, Chen X: **Regulation of N6-methyladenosine (m6A) RNA methylation in microglia-mediated inflammation and ischemic stroke.** *Front Cell Neurosci* 2022, **16:**955222.

22. Chatterjee B, Shen CJ, Majumder P: **RNA Modifications and RNA Metabolism in Neurological Disease Pathogenesis.** *Int J Mol Sci* 2021, **22**.

23. Hill M, Tran N: **Global miRNA to miRNA Interactions: Impacts for miR-21.** *Trends Cell Biol* 2021, **31:**3-5.

24. Ooi JYY, Bernardo BC, Singla S, Patterson NL, Lin RCY, McMullen JR: **Identification of miR-34 regulatory networks in settings of disease and antimiR-therapy: Implications for treating cardiac pathology and other diseases.** *RNA Biol* 2017, **14:**500-513.

25. Wang D, Sun X, Wei Y, Liang H, Yuan M, Jin F, Chen X, Liu Y, Zhang CY, Li L, Zen K: **Nuclear miR-122 directly regulates the biogenesis of cell survival oncomiR miR-21 at the posttranscriptional level.** *Nucleic Acids Res* 2018, **46:**2012-2029.

26. Price AM, Hayer KE, McIntyre ABR, Gokhale NS, Abebe JS, Della Fera AN, Mason CE, Horner SM, Wilson AC, Depledge DP, Weitzman MD: **Direct RNA sequencing reveals m(6)A modifications on adenovirus RNA are necessary for efficient splicing.** *Nat Commun* 2020, **11:**6016.

27. Kashima R, Hata A: **The role of TGF-beta superfamily signaling in neurological disorders.** *Acta Biochim Biophys Sin (Shanghai)* 2018, **50:**106-120.

28. Su C, Miao J, Guo J: **The relationship between TGF-beta1 and cognitive function in the brain.** *Brain Res Bull* 2023, **205:**110820.

29. Deng Z, Fan T, Xiao C, Tian H, Zheng Y, Li C, He J: **TGF-beta signaling in health, disease, and therapeutics.** *Signal Transduct Target Ther* 2024, **9:**61.

30. Agarwal V, Bell GW, Nam JW, Bartel DP: **Predicting effective microRNA target sites in mammalian mRNAs.** *Elife* 2015, **4**.

31. Roberts ES, Burudi EM, Flynn C, Madden LJ, Roinick KL, Watry DD, Zandonatti MA, Taffe MA, Fox HS: **Acute SIV infection of the brain leads to upregulation of IL6 and interferon-regulated genes: expression patterns throughout disease progression and impact on neuroAIDS.** *J Neuroimmunol* 2004, **157:**81-92.

32. Cooper DB, Bunner AE, Kennedy JE, Balldin V, Tate DF, Eapen BC, Jaramillo CA: **Treatment of persistent post-concussive symptoms after mild traumatic brain injury: a systematic review of cognitive rehabilitation and behavioral health interventions in military service members and veterans.** *Brain Imaging Behav* 2015, **9:**403-420.

33. Russo E, Guy GW: **A tale of two cannabinoids: the therapeutic rationale for combining tetrahydrocannabinol and cannabidiol.** *Med Hypotheses* 2006, **66:**234-246.

34. Vermersch P: **Sativex(®) (tetrahydrocannabinol + cannabidiol), an endocannabinoid system modulator: basic features and main clinical data.** *Expert Rev Neurother* 2011, **11:**15-19.

35. Wang H, Song X, Song C, Wang X, Cao H: **m(6)A-seq analysis of microRNAs reveals that the N6-methyladenosine modification of miR-21-5p affects its target expression.** *Arch Biochem Biophys* 2021, **711:**109023.

36. Berulava T, Rahmann S, Rademacher K, Klein-Hitpass L, Horsthemke B: **N6-adenosine methylation in MiRNAs.** *PLoS One* 2015, **10:**e0118438.

37. van den Homberg DAL, van der Kwast R, Quax PHA, Nossent AY: **N-6-Methyladenosine in Vasoactive microRNAs during Hypoxia; A Novel Role for METTL4.** *Int J Mol Sci* 2022, **23**.

38. Lichinchi G, Gao S, Saletore Y, Gonzalez GM, Bansal V, Wang Y, Mason CE, Rana TM: **Dynamics of the human and viral m(6)A RNA methylomes during HIV-1 infection of T cells.** *Nat Microbiol* 2016, **1:**16011.

39. Lichinchi G, Rana TM: **Profiling of N(6)-Methyladenosine in Zika Virus RNA and Host Cellular mRNA.** *Methods Mol Biol* 2019, **1870:**209-218.

40. Lichinchi G, Zhao BS, Wu Y, Lu Z, Qin Y, He C, Rana TM: **Dynamics of Human and Viral RNA Methylation during Zika Virus Infection.** *Cell Host Microbe* 2016, **20:**666-673.

41. Platanias LC: **Mechanisms of type-I- and type-II-interferon-mediated signalling.** *Nat Rev Immunol* 2005, **5:**375-386.

Table 1. Animal IDs, SIV inoculum, duration of infection and viral loads in combination anti-retroviral therapy treated chronic SIV-infected rhesus macaques receiving vehicle or Δ^9-THC :CBD combination

Animal ID	SIV Inoculum	Duration of Infection (days)	12 DPI Plasma viral loads 10^6/mL	Plasma Viral loads at necropsy 10^6/mL	Basal Ganglia viral loads 10^6/mg	Opportunistic Infections
Chronic SIV-Infected, cART and Vehicle treated						
VSART1	SIVmac251	180	2.50	ND	ND	ND
VSART1	SIVmac251	180	5.43	ND	ND	ND
VSART1	SIVmac251	180	1.93	ND	ND	ND
VSART1	SIVmac251	180	2.23	ND	ND	ND
Chronic SIV-Infected, cART and Δ^9-THC:CBD treated						
TCART1	SIVmac251	180	8.2 *	ND	ND	ND
TCART2	SIVmac251	180	15.8 *	ND	ND	ND
TCART3	SIVmac251	180	16.8 #	ND	ND	ND
Uninfected Controls						
Control 1	NA	NA	NA	NA	NA	NA
Control 2	NA	NA	NA	NA	NA	NA
Control 3	NA	NA	NA	NA	NA	NA
Control 4	NA	NA	NA	NA	NA	NA

ND- None detected
NA- Not application
* - 20 DPI viral load
# - 30 DPI viral load
DPI- Days post SIV Infection

Table 2: Total number of identified m^6A methylated miRNAs per group

Infection and treatment groups	Hypomethylated	Hypermethylated	Total modifications
VEH_SIV_cART_vs_Control	1755	50	**1805**
THC-CBD_SIV_cART_vs_Control	1779	26	**1805**
VEH_SIV_cART_vs_THC-CBD_SIV	105	1700	**1805**

Table 3: Number of signi*ficantly* m^6A methylated miRNAs per group	
Infection and treatment groups	**# of m^6A modified miRNA**
Hypo_VEH/SIV/cART_vs_Control	1091
Hyper_VEH/SIV_cART_vs_Control	7
Hypo_THC-CBD/SIV/cART_vs_Control	1575
Hyper_THC-CBD/SIV/cART_vs_Control	2
Hypo_VEH/SIV/cART_vs_THC-CBD/SIV	1
Hyper_VEH/SIV/cART_vs_THC-CBD/SIV	43

Table 4: Top IPA neuroinflammation network molecules

Hypo_VEH_SIV _cART_vs_Control	Hyper_VEH_SIV _cART_vs_Control
ABL1	20s proteasome
AKT2	APBB1
CASP6	ARFIP2
CASP7	BAX
caspase	C5AR1
CAV1	calpain
CDKN1B	CAPN10
CTNNB1	CCR7
ERBB2	CX3CR1
ERBIN	CXCL12
FAK	CXCR1
GJA1	estrogen receptor
HDAC4	FFAR3
Hsp90	GC-GCR dimer
HSPA1A/HSPA1B	GPR17
Importin alpha	GRM3
JAK2	Growth hormone
JINK1/2	H3-3A/H3-3B
lipoxygenase	HCAR1
MAPK7	HIF1A
miR-184	Ldh (complex)
miR-331-3p	MAP1B
miR-548h-5p	MBP
nuclease	MTORC1
PARP	P110
PDLIM7	P2RY13
PGF	PDK4
Rag	Pka
RNA pol II	PTGER3
Rnr	Rac
SMAD4	Ras homolog
TCR	Spectrin
TEAD1	SYN1
TP63	TBP
USP17L	tubulin

Hypo_THC-CBD _SIV_cART_v_Control	Hyper_THC_CBD_SIV _cART_v_Control
ACTA2	ADCY
Actin	ADORA1
ADAM9	ADRB
CAMK2	cacn
CD44	CACNA1E
Cdc42	CACNA2D1
Ck2 alpha	CACNG2
Cofilin	CNR1
ERBB2	CRH
Erm	DAGLA
F Actin	ERK
GLI1	estrogen receptor
GNAI2	Fcgr3
HDAC6	G protein beta gamma
Histone h2a	GALR1
HSP90B1	Girk
Insulin	GRK
ITGB1	HOMER1
miR-200b-3p	HTR1D
miR-216a-5p	IDO
miR-331-3p	Ifn
miR-548h-5p	Ifnar
MYH9	IL12 (complex)
PRKCE	JAK
Proinsulin	LIFR
PTEN	NMUR2
Rap1	NPY5R
RAS	P-type Calcium Channel
SMAD2	p38 Sapk
SMAD3	PDYN
Smad2/3	SLC6A4
TGFBR1	SSTR3
tubulin	STAT
tyrosine kinase	Stat dimer
Wnt	voltage-gated calcium channel

Hypo_VEH_SIV_cART _v_THC_CBD_SIV	Hyper_VEH_SIV_cART _v_THC_CBD_SIV
ADCY	Akt
ADRB3	Alp
APC/APC2	BMPR2
CACNA2D1	calpain
Endothelin	CDKN1B
G protein alpha	collagen
G protein alpha i	Creb
GNRH	Cyclin A
Gpcr	Cyclin E
GPR35	estrogen receptor
GPR37	Hdac
GPR85	Hsp27
GPR89A/GPR89B	ITGA5
IL1B	JINK1/2
ITPR	Lefty
Ldh (complex)	miR-181a-5p
LPAR4	miR-27a-3p
N-type Calcium Channel	miR-92a-3p
NAPB	Mucin
NLGN4X	Osteocalcin
NMDA Receptor	Pdgf (complex)
NRXN1	PDGF BB
Pka	R-Smad
PLC	Rb
PP2A	ROCK
PRLHR	SMAD3
Proinsulin	SMAD4
PTGER4	SMAD5
RXFP1	Smad
RXFP3	SMAD1/5/9
SLC6A4	Smad1/5/8-Smad4
SNAP25	Smad2/3
SSTR2	Smad2/3-Smad4
SSTR3	Tgf beta
voltage-gated calcium channel	TGFBR

Table 5: Top Diseases linked to neuroinflammation network molecules.

Hypo_VEH_SIV_cART_vs_Control	
Diseases	**p-value**
Invasion of cells	1.49E-76
Cell movement of tumor cell lines	7.53E-73
Migration of cells	1.09E-70
Cell proliferation of tumor cell lines	1.33E-69
Migration of tumor cell lines	7.28E-68
Cell movement	2.81E-67
Metastatic solid tumor	3.2E-66
Advanced malignant solid tumor	9.23E-66
Invasion of tumor cell lines	5.93E-65
Apoptosis of tumor cell lines	1.34E-64
Metastasis	4.89E-64
Advanced malignant tumor	5.12E-64
Cell death of tumor cell lines	5.15E-63
Necrosis	8.22E-63
Invasive cancer	8.5E-63
Apoptosis	5.52E-60
Abnormal morphology of mediastinum	3.54E-57
Progressive neurological disorder	3.74E-56
Morphology of cardiovascular system	3.71E-55
Abnormal morphology of heart	5.19E-55

Hypo_THC_CBD_SIV_cART_v_Control	
Diseases	**p-value**
Invasion of cells	2.67E-89
Cell movement of tumor cell lines	8.89E-82
Cell proliferation of tumor cell lines	5.38E-80
Migration of cells	5.74E-78
Cell movement	5.06E-77
Advanced malignant tumor	5.59E-77
Advanced malignant solid tumor	6.3E-77
Migration of tumor cell lines	1.18E-76
Apoptosis of tumor cell lines	1.21E-76
Invasion of tumor cell lines	1.34E-76
Metastasis	1.8E-76
Metastatic solid tumor	8.11E-76
Invasive cancer	2.65E-74
Necrosis	1.23E-73
Cell death of tumor cell lines	3.41E-73
Apoptosis	4.18E-69
Progressive neurological disorder	1.22E-66
Morphology of cardiovascular system	1.79E-61
Morphology of heart	7.78E-61
Cell survival	4.1E-60

Hypo_VEH_SIV_cART_v_THC_CBD_SIV	
Diseases	**p-value**
Weight gain	2.78E-19
Non-malignant disorder	2.88E-18
Morphology of nervous system	7.9E-17
Bleeding	8.47E-17
Necrosis	1.13E-16
Hypertrophy	1.4E-16
Growth of epithelial tissue	4.45E-16
Development of vasculature	4.71E-16
Cell death of epithelial cells	5.99E-16
Benign lesion	6.2E-16
Seizure disorder	1.07E-15
Growth of malignant tumor	1.17E-15
Necrosis of epithelial tissue	1.6E-15
Seizures	2.29E-15
Proliferation of epithelial cells	6.37E-15
Lymphoreticular neoplasm	9.44E-15
Hypertrophy of heart	1.02E-14
Cognitive impairment	1.05E-14
Neurological signs	1.26E-14
Cellular homeostasis	2.66E-14

Hyper_VEH_SIV_cART_vs_Control	
Diseases	**p-value**
Quantity of cells	1.32E-66
Organization of cytoskeleton	5.14E-62
Morphology of nervous system	2.59E-61
Microtubule dynamics	3.83E-60
Proliferation of neural cells	1.33E-57
Organization of cytoplasm	3.66E-57
Development of neural cells	9.77E-57
Neurotransmission	1.29E-56
Movement Disorders	1.04E-55
Development of neurons	1.31E-53
Formation of cellular protrusions	2.5E-53
Proliferation of neuronal cells	6.67E-53
Migration of cells	1.46E-52
Cell movement	1.34E-51
Morphology of nervous tissue	2.21E-51
Morphogenesis of nervous tissue	3.38E-50
Transport of molecule	5.54E-50
Abnormal morphology of nervous sys	3.14E-49
Neuronal cell death	1.12E-48
Necrosis	1.79E-48

Hyper_THC_CBD_SIV_cART_v_Control	
Diseases	**p-value**
Quantity of cells	6.56E-35
Neurotransmission	2.47E-30
Morphology of nervous system	5.56E-30
Transport of molecule	6.49E-30
Sensory disorders	8.73E-29
Activation of cells	1.49E-28
Movement Disorders	2.68E-28
Organization of cytoskeleton	3.99E-27
Development of neurons	6.49E-27
Development of neural cells	7.72E-27
Microtubule dynamics	1.47E-26
Neuronal cell death	4.02E-26
Damage of nervous system	4.55E-26
Proliferation of neural cells	1.09E-25
Abnormal morphology of nervous sys	1.29E-25
Glucose metabolism disorder	1.96E-25
Morphology of nervous tissue	3.99E-25
Endocrine pancreatic dysfunction	4.57E-25
Quantity of neurons	7.62E-25
Skin sensation disturbance	7.77E-25

Hyper_VEH_SIV_cART_v_THC_CBD_SIV	
Diseases	**p-value**
Migration of cells	6.84E-14
Advanced malignant solid tumor	2.19E-12
Invasion of cells	2.2E-12
Angiogenesis	2.88E-12
Proliferation of epithelial cell lines	3.49E-12
Vasculogenesis	8.54E-12
Proliferation of progenitor cells	2.76E-11
Advanced malignant tumor	4.8E-11
Proliferation of hematopoietic progenitor cells	8.05E-11
Advanced extracranial solid tumor	2.45E-10
Abnormal morphology of cardio system	2.45E-10
Apoptosis of B-lymphocyte derived cell lines	2.57E-10
Hepatocellular carcinoma	2.76E-10
Survival of organism	2.77E-10
Invasion of tumor cell lines	3.04E-10
Maturation of connective tissue cells	3.05E-10
Invasive cancer	4.11E-10
Connective or soft tissue tumor	4.53E-10
Metastasis	5.22E-10
Metastatic solid tumor	5.73E-10

Table 6: The number of significantly altered miRNAs that were significantly m^6A modified		
Treatment Group	**Total # of significantly m^6A modified miRNA**	**# of miRNAs m^6A modified miRNA with significant change in expression**
Hypo_VEH/SIV/cART_vs_Control	1091 miRNAs	537 (49%) significantly changed. 2 (0.4%) up; 535 (99.6%) down.
Hyper_VEH/SIV/cART_vs_Control	7 miRNAs	5 (71%) miRNAs significantly changed. All (100%) up.
Hypo_THC-CBD/SIV/cART_vs_Control	1575 miRNA	1488 (94%) significantly changed. All (100%) down.
Hyper_THC-CBD/SIV/cART_vs_Control	2 miRNAs	2 (100%) significantly changed (1 (50%) up; 1 (50%) down).
Hypo_VEH/SIV/cART_vs_THC-CBD/SIV/cART	1 miRNA	0
Hyper_VEH/SIV/cART_vs_THC-CBD/SIV/cART	44 miRNAs	35 (80%) significantly changed. All (100%) down.

Table 7: Target genes of miRNAs related to neurotransmitters/other nervous system and pathogen influenced signaling pathways.

Hypo_VEH_SIV _cART_vs_Control	Hyper_VEH_SIV _cART_vs_Control	Hypo_THC-CBD _SIV_cART_v_Control	Hyper_THC_CBD_SIV _cART_v_Control	Hypo_VEH_SIV_cART _v_THC_CBD_SIV	Hyper_VEH_SIV_cART _v_THC_CBD_SIV
ACVR2A	AGER	ACVR1C	ADORA1	FOS	ATF2
AGER	ATF2	APH1A	CD40		BCL2
AKT2	BACE1	B2M	GDNF		BIRC5
APH1B	CALB2	BACE1	GRIN2B		BMPR2
B2M	CASP3	BCL2	HLA-DMA		CALB1
BACE1	CASP8	BDNF	HLA-DPA1		CASP8
BCL2	CCL5	BIRC3			CCL2
BDNF	CD40	CALB2			CCL5
BIRC5	CD80	CASP3			CHP1
CALB2	CD86	CCL2			CNTF
CCL2	CD200	CCL3			CREB3L3
CD80	CD200R1	CD80			CTNNB1
CD86	CHP1	CD86			CXCL10
CHP1	CNTF	CD200R1			CXCL12
CNTF	CX3CR1	CREB3L1			FASLG
CREB1	CXCL12	CREB3L3			GABRA1
CREB3L1	CYBB	CSF1R			GABRA4
CREB3L2	FAS	CX3CL1			GABRB1
CX3CL1	FASLG	CX3CR1			GABRQ
CX3CR1	GABRA3	CXCL10			GRIA1
CXCL10	GABRA4	CXCL12			GRIN1
GABRA1	GABRE	ELP1			GRIN2B
GABRA3	GABRQ	FAS			GRIN2D
GABRA4	GABRR1	FASLG			HLA-DMA
GABRA6	GABRR3	GABRA1			HLA-DMB
GABRB1	GDNF	GABRA3			HLA-DOB
GABRD	GJB1	GABRA4			HLA-DQA1
GABRG2	GRIN2B	GABRA5			HLA-DQB2
GJB1	H2-Eb2	GABRB1			HLA-DRB1
GRIN1	HLA-A	GABRD			ICAM1
GRIN2A	HLA-DMA	GABRG2			IFNA1/IFNA13
GRIN2B	HLA-DPA1	GDNF			IFNG
HLA-B	HLA-E	GJB1			IKBKB
HLA-DPA1	IFNA4	GRIN1			IL34
HLA-DPB1	IFNGR2	GRIN2A			IL12A
HLA-DQA2	IKBKB	GRIN2B			IL12B
HLA-DRA	IKBKE	GRIN2D			IRAK1
HLA-G	IL18	GRINA			KCNJ5
HMGB1	IRAK3	HLA-B			KCNJ6
IFNGR2	JUN	HLA-DQA2			MAP2K4
IL18	KCNJ3	HLA-DRA			MAPK1
JUN	KCNJ5	HLA-G			MAPK4
KCNJ5	KCNJ9	HMOX1			MAPK14
MAP2K4	KLK3	IL6			NFKB2
MAPK1	MAPK4	IL10			NLRP3
MAPK4	MAPK10	IRAK1			NOS2
MAPK8	MAPK14	IRAK2			PIK3C2G

MAPK13 MAPK14 MAPT MFGE8 MYD88 NFATC1 NFATC2 PIK3R2 PLA2G6 PLA2G2D PLA2G2F PLA2G4E PLA2G4F PPP3CC PPP3R2 PYCARD RAC2 RELA SLC6A11 STAT1 TGFB1 TGFBR2 TNF TNFRSF1A WNT1	MAPT NFATC2 PLA2G3 PLA2G2D PLA2G2E PLA2G2F PLA2G4F PLCG1 PPP3CB PPP3R2 S100G TGFB1 TGFBR1 TICAM1 TIRAP TLR10 Tlr13 ZBTB12	KCNJ6 MAPK1 MAPK4 MAPK6 MAPK8 MAPK12 MAPK14 MAPT MFGE8 MYD88 NFATC2 NGF PLA2G3 PLA2G2D PLA2G2F PLA2G4F PPP3CA PPP3CC PPP3R2 PRKCG PSENEN PTGS2 PYCARD RAC1 RAC2 S100B SLC6A1 SNCA STAT1 TGFB1 TGFB2 TGFBR1 TGFBR2 TGFBR3 TICAM1 TLR4 TNF TNFRSF1A WNT1			PIK3R3 PLA2G1B PLA2G4B PLA2G4C PSEN1 RAC3 S100B SLC6A1 STAT1 TGFB2 TICAM1 TIRAP TLR10 VCAM1

Table 8: Potential biological functions of the m6A methylated miRNA targets

Pathways	Hypo_VEH_SIV_cART_vs_Control	Hyper_VEH_SIV_cART_vs_Control	Hypo_THC-CBD_SIV_cART_v_Control	Hyper_THC_CBD_SIV_cART_v_Control	Hypo_VEH_SIV_cART_v_THC_CBD_SIV	Hyper_VEH_SIV_cART_v_THC_CBD_SIV
GO Biological Process	Cellular response to anisomycin Positive regulation of dendritic cell differentiation Negative regulation of hippocampal neuron apoptotic process Langerhans cell differentiation Regulation of retinal cell programmed cell death	Cellular response to anisomycin Positive regulation of CD8-positive, alpha-beta T cell proliferation Negative regulation of calcium ion import across plasma membrane Membrane repolarization during atrial cardiac muscle cell action potential Positive regulation of dopamine secretion	Negative regulation of interleukin-23 production Negative regulation of alkaline phosphatase activity Regulation of chronic inflammatory response to antigenic stimulus Chronic inflammatory response to antigenic stimulus Negative regulation of calcium ion import across plasma membrane		Response to gravity Integrated stress response signaling Response to corticosterone Response to progesterone Positive regulation of osteoclast differentiation	Negative regulation of MET in metanephros morphogenesis Regulation of retinal cell programmed cell death Retinal cell programmed cell death Regulation of core promoter binding Peptide antigen assembly with MHC class II protein complex
GO Molecular Function	Benzodiazepine receptor activity CX3C chemokine receptor binding Glutamate-gated calcium ion channel activity Type III transforming growth factor beta receptor binding GABA-gated chloride ion channel activity	G-protein activated inward rectifier potassium channel activity Glycosylated region protein binding IkappaB kinase activity Voltage-gated potassium channel activity (atrial cardiac muscle repolarization) Mitogen-activated protein kinase p38 binding	Glutamate-gated calcium ion channel activity Type III transforming growth factor beta receptor binding CX3C chemokine receptor binding NMDA glutamate receptor activity Benzodiazepine receptor activity		cAMP response element binding R-SMAD binding Transcription coregulator binding DNA-binding transcription activator activity, RNA polymerase II-specific RNA polymerase II-specific DNA-binding transcription factor bi	interleukin-12 binding interleukin-12 receptor binding Glutamate-gated calcium ion channel activity G-protein activated inward rectifier potassium channel activity MHC class II receptor activity
GO Cellular Component	Transforming growth factor beta ligand-receptor complex Transcription factor AP-1 complex MHC class I protein complex GABA-A receptor complex NMDA selective glutamate receptor complex	Transforming growth factor beta ligand-receptor complex Transcription factor AP-1 complex Death-inducing signaling complex Ripoptosome CD95 death-inducing signaling complex	Transforming growth factor beta complex Transforming growth factor beta ligand-receptor complex Calcineurin complex NMDA selective glutamate receptor complex GABA-A receptor complex	MHC class II protein complex Plasma membrane protein complex Cell surface	Transcription factor AP-1 complex Euchromatin RNA polymerase II transcription regulator complex Transcription regulator complex protein-DNA complex	interleukin-12 complex MHC class II protein complex NMDA selective glutamate receptor complex Ripoptosome interleukin-12 receptor complex
KEGG Pathways	Allograft rejection Graft-versus-host disease Nicotine addiction Type I diabetes mellitus alpha-Linolenic acid metabolism	Allograft rejection Graft-versus-host disease Type I diabetes mellitus Autoimmune thyroid disease alpha-Linolenic acid metabolism	Allograft rejection Graft-versus-host disease Nicotine addiction Type I diabetes mellitus Chagas disease	Asthma Allograft rejection Intestinal immune network for IgA production Autoimmune thyroid disease Graft-versus-host disease	Osteoclast differentiation Amphetamine addiction Cocaine addiction IL-17 signaling pathway Th1 and Th2 cell differentiation	Allograft rejection Nicotine addiction Type I diabetes mellitus Leishmaniasis Graft-versus-host disease
Reactome Pathways	TGFBR2 MSI Frameshift Mutants in Cancer TGFBR2 Kinase Domain Mutants in Cancer TGFBR1 LBD Mutants in Cancer Activation of the AP-1 family of transcription factors CLEC7A/inflammasome pathway	TGFBR2 Kinase Domain Mutants in Cancer FasL/ CD95L signaling TGFBR1 LBD Mutants in Cancer Activation of the AP-1 family of transcription factors TLR3-mediated TICAM1-dependent programmed cell death	TGFBR2 Kinase Domain Mutants in Cancer TGFBR2 MSI Frameshift Mutants in Cancer TGFBR1 LBD Mutants in Cancer TGFBR1 KD Mutants in Cancer SMAD2/3 Phosphorylation Motif Mutants in Cancer		Activation of the AP-1 family of transcription factors NGF-stimulated transcription MAPK targets/ Nuclear events mediated by MAP kinases Estrogen-dependent nuclear events downstream of ESR-membrane signaling FCERI mediated MAPK activation	FasL/ CD95L signaling Activation of the AP-1 family of transcription factors TLR3-mediated TICAM1-dependent programmed cell death IkBA variant leads to EDA-ID TRIF-mediated programmed cell death
WikiPathways	Suppression of HMGB1 mediated inflammation by THBD Neuroinflammation LDL- influence on CD14 and TLR4 Activation of NLRP3 inflammasome by SARS-CoV-2 mBDNF and proBDNF regulation of GABA neurotransmission	Control of immune tolerance by vasoactive intestinal peptide Cell interactions of the pancreatic cancer microenvironment Apoptosis modulation by HSP70 Suppression of HMGB1 mediated inflammation by THBD Nod-like receptor (NLR) signaling pathway	Cell interactions of the pancreatic cancer microenvironment COVID-19 adverse outcome pathway Control of immune tolerance by vasoactive intestinal peptide LDL- influence on CD14 and TLR4 IL-10 anti-inflammatory signaling pathway	Allograft rejection	Estrogen signaling pathway Neuroinflammation MFAP5-mediated ovarian cancer cell motility and invasiveness Estrogen receptor pathway Mammary gland development pathway - Puberty (Stage 2 of 4)	Platelet-mediated interactions with vascular and circulating cells ApoE and miR-146 in inflammation and atherosclerosis Cell interactions of the pancreatic cancer microenvironment Ebstein-Barr virus LMP1 signaling IL1 and megakaryocytes in obesity
Disease-gene associations	Granulomatosis with polyangiitis Myxofibrosarcoma Takayasus arteritis Stevens-Johnson syndrome Childhood absence epilepsy	Schizoaffective disorder Autoimmune lymphoproliferative syndrome Cognitive disorder Arthritis Lower respiratory tract disease	Bacterial sepsis Takayasus arteritis Adult respiratory distress syndrome Bronchitis Picks disease			Leukostasis Sjogrens syndrome Rosacea Pemphigus vulgaris Schizoaffective disorder
Tissue expression	U-937 cell Monocyte-derived dendritic cell SH-SY5Y cell Cerebral cortical neuron Bone marrow-derived dendritic cell	Bone marrow-derived dendritic cell PC-3 cell Monocyte-derived dendritic cell SH-SY5Y cell Sciatic nerve	Olfactory ensheathing cell Palatine uvula SH-SY5Y cell U-937 cell Peritoneal macrophage		Nucleus preopticus medialis Lateral ventricle Chronic lymphocytic leukemia cell Cervical carcinoma cell Leukemia cell	Human aortic endothelial cell Venule Blood vessel wall Vascular cell Entorhinal cortex

Table 9: 14 miRNAs that were m^6A hypermethylated bearing RRACH or DRACH motif					
Mature-ID	**Sequence**	**Fold Change**	**Log_2 Fold Change**	**P value (unpaired t-test)**	**FDR**
hsa-miR-6806-3p	UGAAGCUCUGACAUUCCUGCAG	3.21	1.68	0.02	0.63
hsa-miR-154-3p	AAUCAUACACGGUUGACCUAUU	3.11	1.64	0.02	0.63
hsa-miR-4671-5p	ACCGAAGACUGUGCGCUAAUCU	2.12	1.08	0.02	0.63
hsa-miR-873-3p	GGAGACUGAUGAGUUCCCGGGA	2.03	1.02	0.02	0.63
hsa-miR-6776-3p	CAACCACCACUGUCUCUCCCCAG	2.01	1.00	0.03	0.63
hsa-miR-4285	GCGGCGAGUCCGACUCAU	1.93	0.95	0.05	0.63
hsa-miR-6857-3p	UGACUGAGCUUCUCCCCACAG	1.88	0.91	0.02	0.63
hsa-miR-6764-3p	UCUCUGGUCUUUCCUUGACAG	1.75	0.81	0.01	0.63
hsa-miR-4803	UAACAUAAUAGUGUGGAUUGA	1.74	0.80	0.03	0.63
hsa-miR-6759-3p	UGACCUUUGCCUCUCCCCUCAG	1.70	0.77	0.04	0.63
hsa-miR-3135a	UGCCUAGGCUGAGACUGCAGUG	1.63	0.71	0.02	0.63
hsa-miR-8059	GGGGAACUGUAGAUGAAAAGGC	1.58	0.66	0.04	0.63
hsa-miR-181c-5p	AACAUUCAACCUGUCGGUGAGU	1.51	0.60	0.02	0.63
hsa-miR-181a-5p	AACAUUCAACGCUGUCGGUGAGU	1.51	0.60	0.01	0.63

Table 10: Basal ganglia tissue m^6A-enriched miRNAs present in Extracellular Vesicles (EVs)	
Pathways	**Processes**
GO Biological Process	Uterine wall breakdown Negative regulation of interleukin-23 production Positive regulation of EMT involved in endocardial cushion formation Positive regulation of tight junction disassembly Positive regulation of calcidiol 1-monooxygenase activity
GO Molecular Function	Type III transforming growth factor beta receptor binding Interleukin-12 receptor binding Interleukin-12 binding Activin receptor activity, type I Activin receptor activity
GO Cellular Component	Transforming growth factor beta complex Interleukin-12 complex Transforming growth factor beta ligand-receptor complex Activin receptor complex Interleukin-12 receptor complex
KEGG Pathways	Allograft rejection African trypanosomiasis alpha-Linolenic acid metabolism Type I diabetes mellitus Leishmaniasis
Reactome Pathways	TGFBR2 Kinase Domain Mutants in Cancer TGFBR2 MSI Frameshift Mutants in Cancer TGFBR1 LBD Mutants in Cancer TGFBR1 KD Mutants in Cancer SMAD2/3 Phosphorylation Motif Mutants in Cancer
WikiPathways	Nanomaterial-induced inflammasome activation COVID-19 adverse outcome pathway TCA cycle nutrient use and invasiveness of ovarian cancer Platelet-mediated interactions with vascular and circulating cells LTF danger signal response pathway
Disease-gene associations	Silicosis Adult-onset Stills disease Loeys-Dietz syndrome Adult respiratory distress syndrome Muckle-Wells syndrome
Tissue expression	U-937 cell Ankle joint Palatine uvula J-774A.1 cell J-774 cell

Table 11: Gene list involved in functional categories shown in Figure 6F

Extrinsic apoptotic signaling pathway	Leukocyte proliferation	Positive regulation of response to external stimulus	Neuron death	Response to molecule of bacterial origin	Positive regulation of cell activation	Regulation of cell-cell adhesion	T cell activation	Regulation of leukocyte activation	Positive regulation of cell motility
ACVR1	AGER	AGER	BACE1	CASP1	AGER	AGER	AGER	AGER	ACVR1
BCL2	BCL2	BMPR2	BCL2	CASP3	BCL2	CASP3	BCL2	BCL2	BCL2
CASP3	CASP3	CCL3	BDNF	CCL2	CCL2	CCL2	CASP3	CASP3	BMPR2
FAS	HLA-E	CXCL10	CASP3	CCL3	HLA-E	CXCL12	CCL2	CCL2	CCL3
FASLG	IFNA4	CXCL12	CCL2	CXCL10	IL10	HLA-E	HLA-E	HLA-E	CXCL10
HMOX1	IL10	HLA-E	CCL3	FASLG	IL12A	IL10	IFNA4	HMOX1	CXCL12
IL12A	IL12A	IL12A	CD200R1	IL10	IL12B	IL12A	IL10	IL10	ELP1
IL1B	IL12B	IL12B	CHP1	IL12A	IL18	IL12B	IL12A	IL12A	HMOX1
IL6R	IL18	IL18	FASLG	IL12B	IL1B	IL18	IL12B	IL12B	IL12A
JAK2	IL1B	IL1B	GABRA5	IL18	IL6R	IL1B	IL18	IL18	IL1B

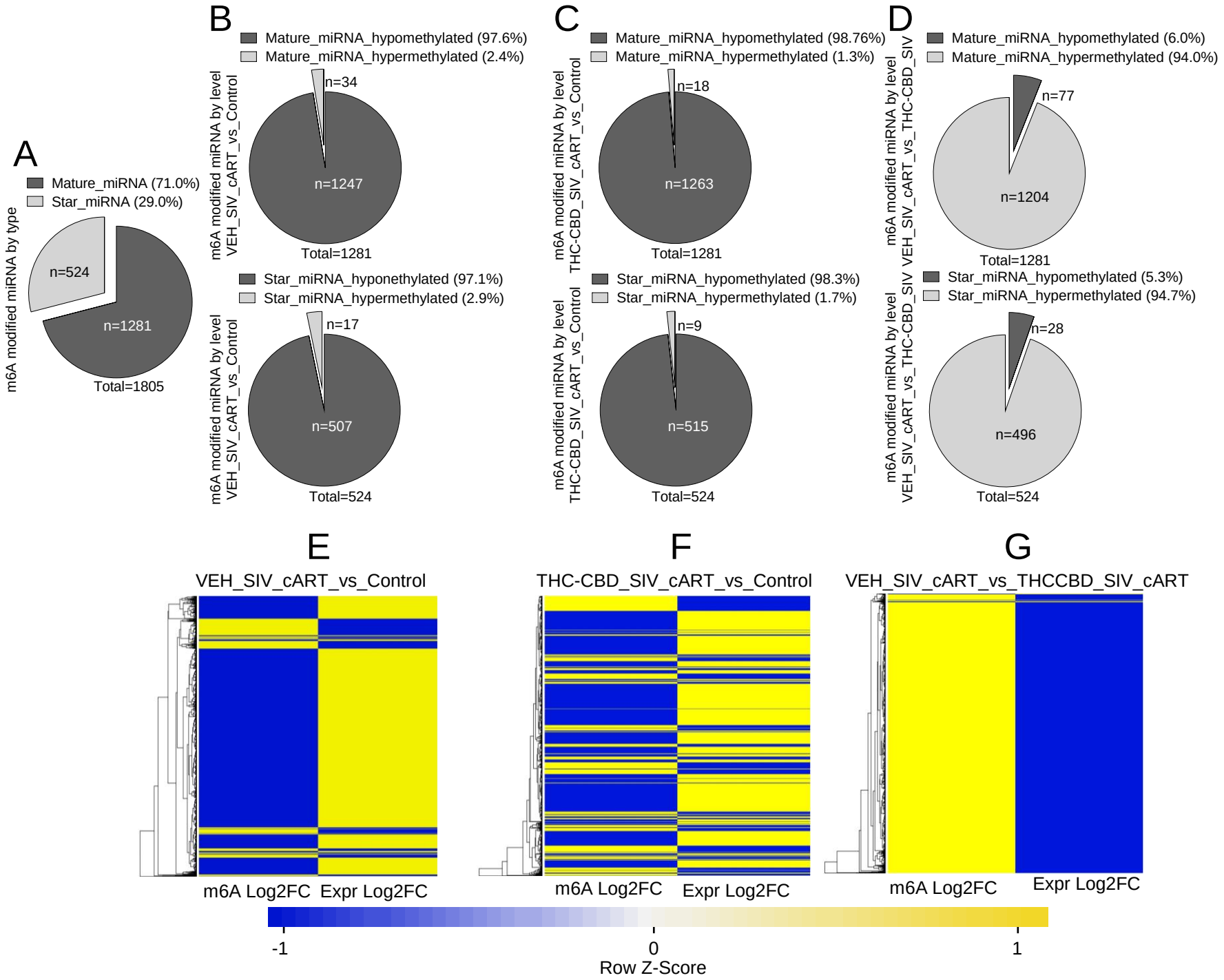
A
m6A modified miRNA by type
Mature_miRNA (71.0%)
Star_miRNA (29.0%)
n=524
n=1281
Total=1805
B
m6A modified miRNA by level
VEH_SIV_cART_vs_Control
Mature_miRNA_hypomethylated (97.6%)
Mature_miRNA_hypermethylated (2.4%)
n=34
n=1247
Total=1281
Star_miRNA_hyponethylated (97.1%)
Star_miRNA_hypermethylated (2.9%)
n=17
n=507
Total=524
C
m6A modified miRNA by level
THC-CBD_SIV_cART_vs_Control
Mature_miRNA_hypomethylated (98.76%)
Mature_miRNA_hypermethylated (1.3%)
n=18
n=1263
Total=1281
Star_miRNA_hypomethylated (98.3%)
Star_miRNA_hypermethylated (1.7%)
n=9
n=515
Total=524
D
m6A modified miRNA by level
VEH_SIV_cART_vs_THC-CBD_SIV
Mature_miRNA_hypomethylated (6.0%)
Mature_miRNA_hypermethylated (94.0%)
n=77
n=1204
Total=1281
Star_miRNA_hypomethylated (5.3%)
Star_miRNA_hypermethylated (94.7%)
n=28
n=496
Total=524
E
VEH_SIV_cART_vs_Control
m6A Log2FC
Expr Log2FC
F
THC-CBD_SIV_cART_vs_Control
m6A Log2FC
Expr Log2FC
G
VEH_SIV_cART_vs_THCCBD_SIV_cART
m6A Log2FC
Expr Log2FC
-1
0
1
Row Z-Score

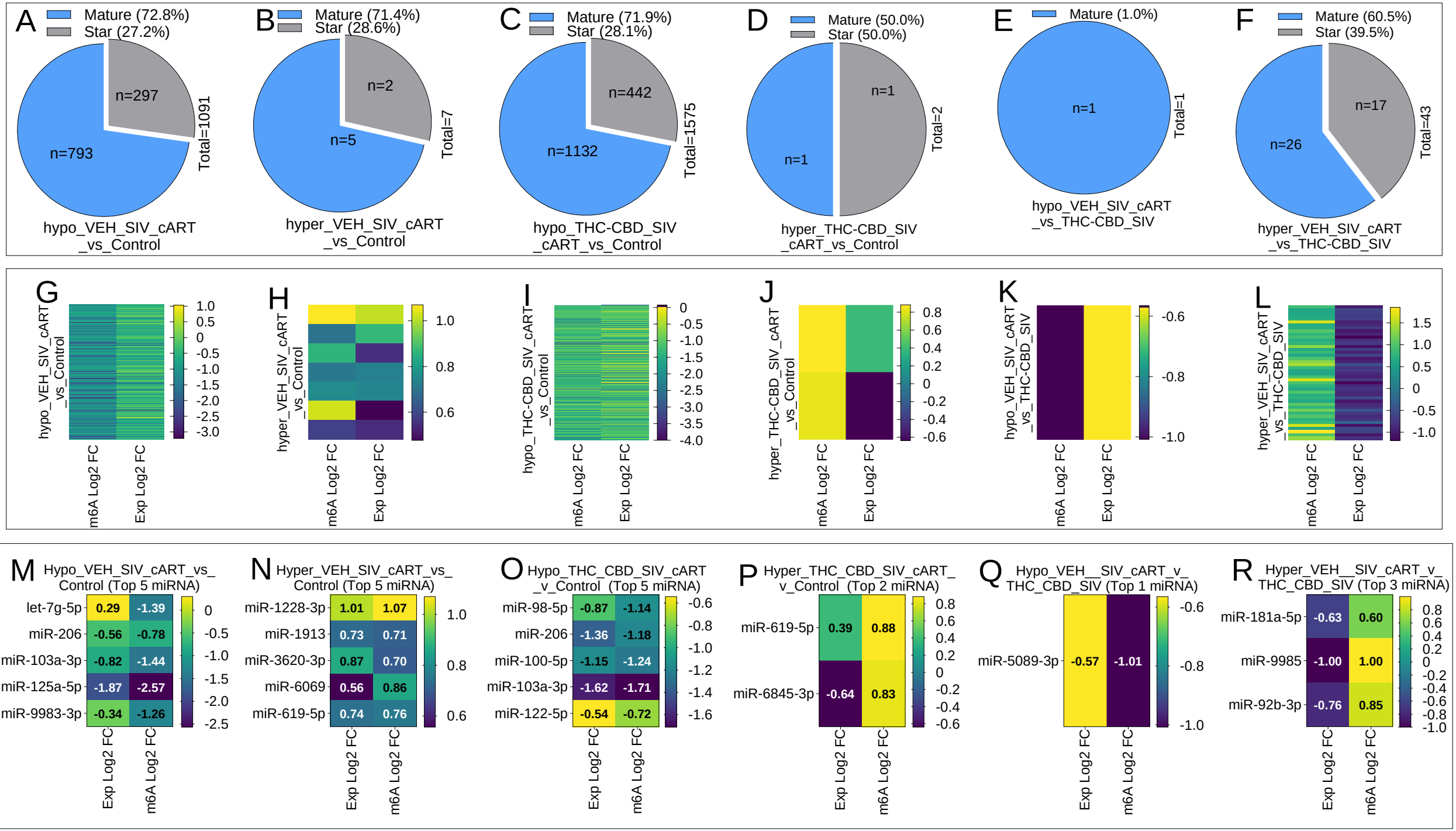
A
Mature (72.8%)
Star (27.2%)
n=297
n=793
Total=1091
hypo_VEH_SIV_cART _vs_Control
B
Mature (71.4%)
Star (28.6%)
n=2
n=5
Total=7
hyper_VEH_SIV_cART _vs_Control
C
Mature (71.9%)
Star (28.1%)
n=442
n=1132
Total=1575
hypo_THC-CBD_SIV _cART_vs_Control
D
Mature (50.0%)
Star (50.0%)
n=1
n=1
Total=2
hyper_THC-CBD_SIV _cART_vs_Control
E
Mature (1.0%)
n=1
Total=1
hypo_VEH_SIV_cART _vs_THC-CBD_SIV
F
Mature (60.5%)
Star (39.5%)
n=17
n=26
Total=43
hyper_VEH_SIV_cART _vs_THC-CBD_SIV
G
hypo_VEH_SIV_cART _vs_Control
m6A Log2 FC
Exp Log2 FC
H
hyper_VEH_SIV_cART _vs_Control
m6A Log2 FC
Exp Log2 FC
I
hypo_THC-CBD_SIV_cART _vs_Control
m6A Log2 FC
Exp Log2 FC
J
hyper_THC-CBD_SIV_cART _vs_Control
m6A Log2 FC
Exp Log2 FC
K
hypo_VEH_SIV_cART _vs_THC-CBD_SIV
m6A Log2 FC
Exp Log2 FC
L
hyper_VEH_SIV_cART _vs_THC-CBD_SIV
m6A Log2 FC
Exp Log2 FC
M
Hypo_VEH_SIV_cART_vs_ Control (Top 5 miRNA)
let-7g-5p 0.29 -1.39
miR-206 -0.56 -0.78
miR-103a-3p -0.82 -1.44
miR-125a-5p -1.87 -2.57
miR-9983-3p -0.34 -1.26
Exp Log2 FC
m6A Log2 FC
N
Hyper_VEH_SIV_cART_vs_ Control (Top 5 miRNA)
miR-1228-3p 1.01 1.07
miR-1913 0.73 0.71
miR-3620-3p 0.87 0.70
miR-6069 0.56 0.86
miR-619-5p 0.74 0.76
Exp Log2 FC
m6A Log2 FC
O
Hypo_THC_CBD_SIV_cART _v_Control (Top 5 miRNA)
miR-98-5p -0.87 -1.14
miR-206 -1.36 -1.18
miR-100-5p -1.15 -1.24
miR-103a-3p -1.62 -1.71
miR-122-5p -0.54 -0.72
Exp Log2 FC
m6A Log2 FC
P
Hyper_THC_CBD_SIV_cART_ v_Control (Top 2 miRNA)
miR-619-5p 0.39 0.88
miR-6845-3p -0.64 0.83
Exp Log2 FC
m6A Log2 FC
Q
Hypo_VEH__SIV_cART_v_ THC_CBD_SIV (Top 1 miRNA)
miR-5089-3p -0.57 -1.01
Exp Log2 FC
m6A Log2 FC
R
Hyper_VEH__SIV_cART_v_ THC_CBD_SIV (Top 3 miRNA)
miR-181a-5p -0.63 0.60
miR-9985 -1.00 1.00
miR-92b-3p -0.76 0.85
Exp Log2 FC
m6A Log2 FC

Neuroinflammation networks

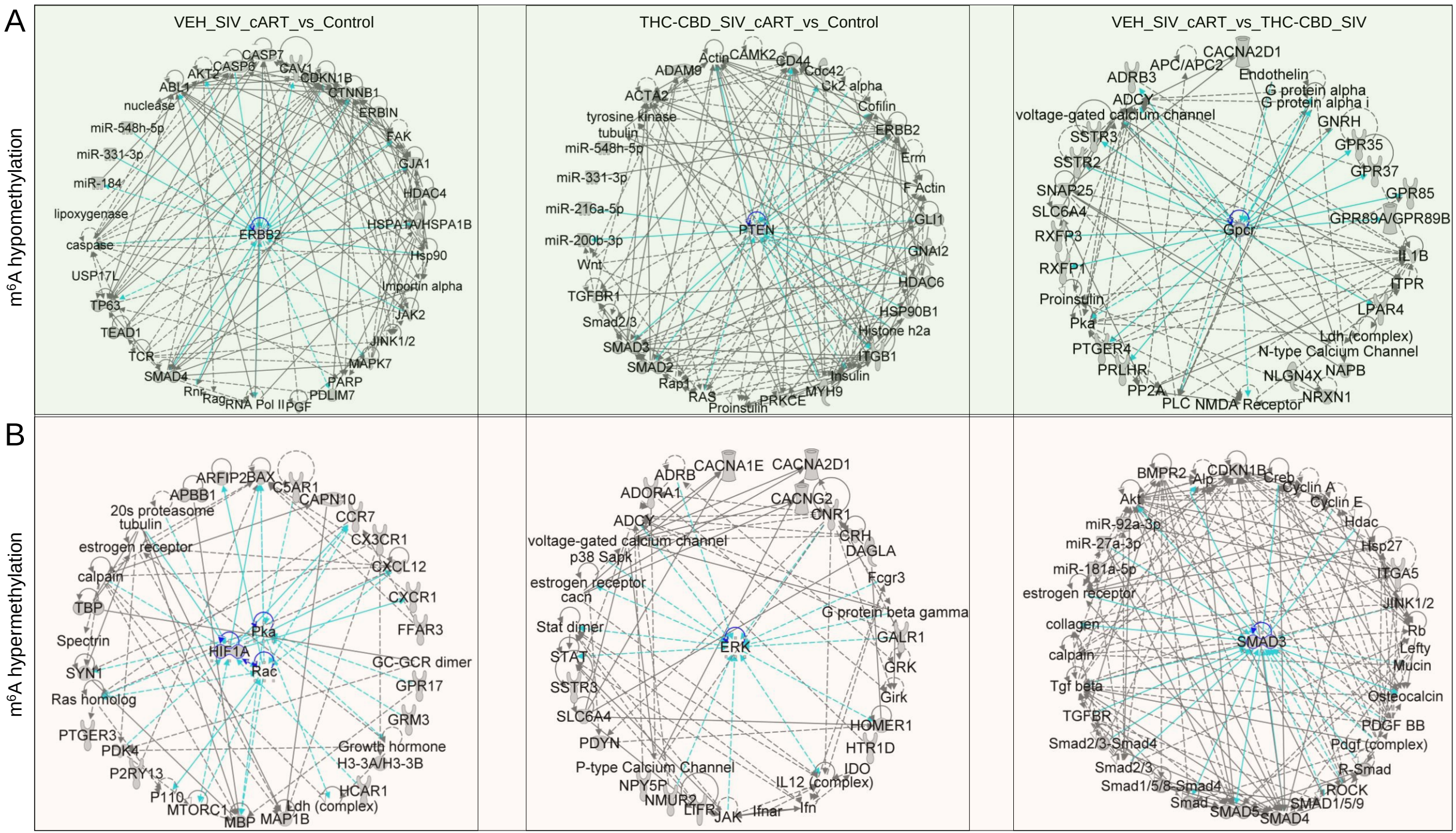

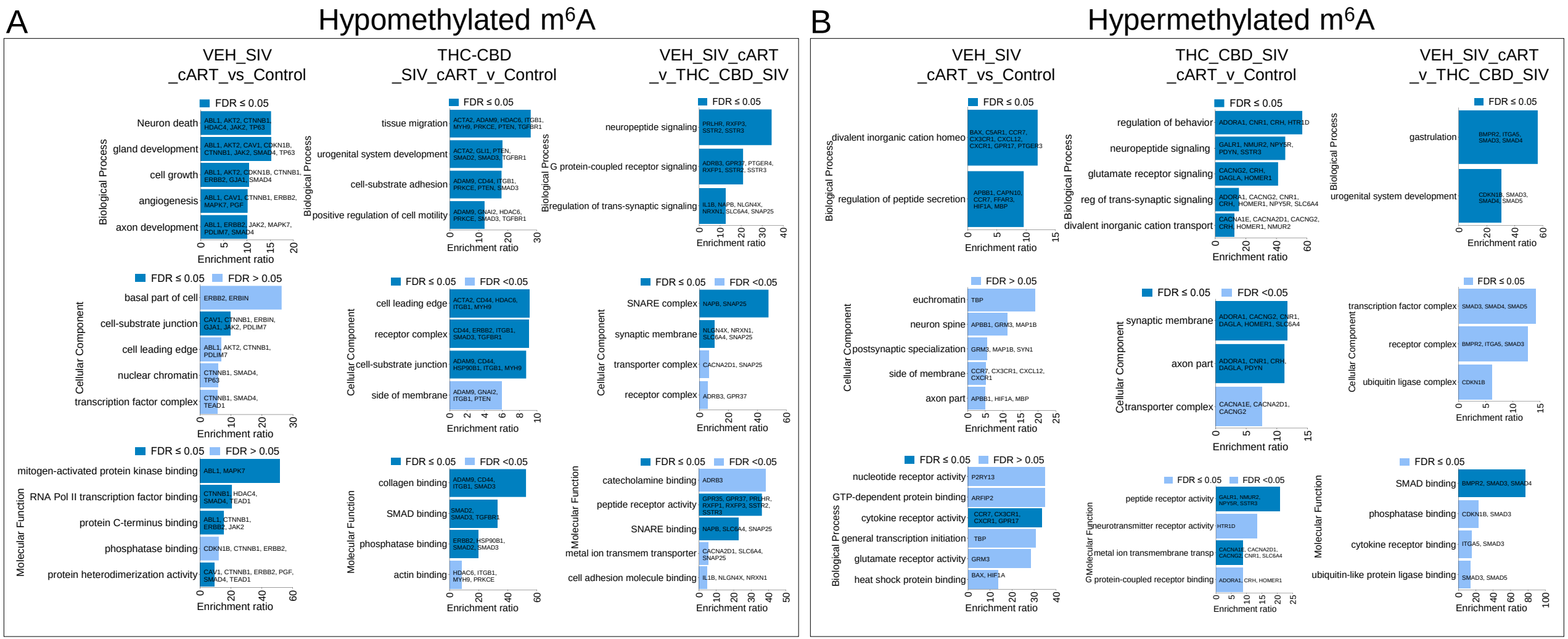
A
Hypomethylated m6A
VEH_SIV _cART_vs_Control
THC-CBD _SIV_cART_v_Control
VEH_SIV_cART _v_THC_CBD_SIV
FDR ≤ 0.05
FDR > 0.05
FDR <0.05
Biological Process
Neuron death
ABL1, AKT2, CTNNB1, HDAC4, JAK2, TP63
gland development
ABL1, AKT2, CAV1, CDKN1B, CTNNB1, JAK2, SMAD4, TP63
cell growth
ABL1, AKT2, CDKN1B, CTNNB1, ERBB2, GJA1, SMAD4
angiogenesis
ABL1, CAV1, CTNNB1, ERBB2, MAPK7, PGF
axon development
ABL1, ERBB2, JAK2, MAPK7, PDLIM7, SMAD4
tissue migration
ACTA2, ADAM9, HDAC6, ITGB1, MYH9, PRKCE, PTEN, TGFBR1
urogenital system development
ACTA2, GLI1, PTEN, SMAD2, SMAD3, TGFBR1
cell-substrate adhesion
ADAM9, CD44, ITGB1, PRKCE, PTEN, SMAD3
positive regulation of cell motility
ADAM9, GNAI2, HDAC6, PRKCE, SMAD3, TGFBR1
neuropeptide signaling
PRLHR, RXFP3, SSTR2, SSTR3
G protein-coupled receptor signaling
ADRB3, GPR37, PTGER4, RXFP1, SSTR2, SSTR3
regulation of trans-synaptic signaling
IL1B, NAPB, NLGN4X, NRXN1, SLC6A4, SNAP25
Enrichment ratio
Cellular Component
basal part of cell
ERBB2, ERBIN
cell-substrate junction
CAV1, CTNNB1, ERBIN, GJA1, JAK2, PDLIM7
cell leading edge
ABL1, AKT2, CTNNB1, PDLIM7
nuclear chromatin
CTNNB1, SMAD4, TP63
transcription factor complex
CTNNB1, SMAD4, TEAD1
cell leading edge
ACTA2, CD44, HDAC6, ITGB1, MYH9
receptor complex
CD44, ERBB2, ITGB1, SMAD3, TGFBR1
cell-substrate junction
ADAM9, CD44, HSP90B1, ITGB1, MYH9
side of membrane
ADAM9, GNAI2, ITGB1, PTEN
SNARE complex
NAPB, SNAP25
synaptic membrane
NLGN4X, NRXN1, SLC6A4, SNAP25
transporter complex
CACNA2D1, SNAP25
receptor complex
ADRB3, GPR37
Molecular Function
mitogen-activated protein kinase binding
ABL1, MAPK7
RNA Pol II transcription factor binding
CTNNB1, HDAC4, SMAD4, TEAD1
protein C-terminus binding
ABL1, CTNNB1, ERBB2, JAK2
phosphatase binding
CDKN1B, CTNNB1, ERBB2,
protein heterodimerization activity
CAV1, CTNNB1, ERBB2, PGF, SMAD4, TEAD1
collagen binding
ADAM9, CD44, ITGB1, SMAD3
SMAD binding
SMAD2, SMAD3, TGFBR1
phosphatase binding
ERBB2, HSP90B1, SMAD2, SMAD3
actin binding
HDAC6, ITGB1, MYH9, PRKCE
catecholamine binding
ADRB3
peptide receptor activity
GPR35, GPR37, PRLHR, RXFP1, RXFP3, SSTR2, SSTR3
SNARE binding
NAPB, SLC6A4, SNAP25
metal ion transmem transporter
CACNA2D1, SLC6A4, SNAP25
cell adhesion molecule binding
IL1B, NLGN4X, NRXN1
B
Hypermethylated m6A
VEH_SIV _cART_vs_Control
THC_CBD_SIV _cART_v_Control
VEH_SIV_cART _v_THC_CBD_SIV
divalent inorganic cation homeo
BAX, C5AR1, CCR7, CX3CR1, CXCL12, CXCR1, GPR17, PTGER3
regulation of peptide secretion
APBB1, CAPN10, CCR7, FFAR3, HIF1A, MBP
regulation of behavior
ADORA1, CNR1, CRH, HTR1D
neuropeptide signaling
GALR1, NMUR2, NPY5R, PDYN, SSTR3
glutamate receptor signaling
CACNG2, CRH, DAGLA, HOMER1
reg of trans-synaptic signaling
ADORA1, CACNG2, CNR1, CRH, HOMER1, NPY5R, SLC6A4
divalent inorganic cation transport
CACNA1E, CACNA2D1, CACNG2, CRH, HOMER1, NMUR2
gastrulation
BMPR2, ITGA5, SMAD3, SMAD4
urogenital system development
CDKN1B, SMAD3, SMAD4, SMAD5
euchromatin
TBP
neuron spine
APBB1, GRM3, MAP1B
postsynaptic specialization
GRM3, MAP1B, SYN1
side of membrane
CCR7, CX3CR1, CXCL12, CXCR1
axon part
APBB1, HIF1A, MBP
synaptic membrane
ADORA1, CACNG2, CNR1, DAGLA, HOMER1, SLC6A4
axon part
ADORA1, CNR1, CRH, DAGLA, PDYN
transporter complex
CACNA1E, CACNA2D1, CACNG2
transcription factor complex
SMAD3, SMAD4, SMAD5
receptor complex
BMPR2, ITGA5, SMAD3
ubiquitin ligase complex
CDKN1B
nucleotide receptor activity
P2RY13
GTP-dependent protein binding
ARFIP2
cytokine receptor activity
CCR7, CX3CR1, CXCR1, GPR17
general transcription initiation
TBP
glutamate receptor activity
GRM3
heat shock protein binding
BAX, HIF1A
peptide receptor activity
GALR1, NMUR2, NPY5R, SSTR3
neurotransmitter receptor activity
HTR1D
metal ion transmembrane transp
CACNA1E, CACNA2D1, CACNG2, CNR1, SLC6A4
protein-coupled receptor binding
ADORA1, CRH, HOMER1
SMAD binding
BMPR2, SMAD3, SMAD4
phosphatase binding
CDKN1B, SMAD3
cytokine receptor binding
ITGA5, SMAD3
ubiquitin-like protein ligase binding
SMAD3, SMAD5
Enrichment ratio

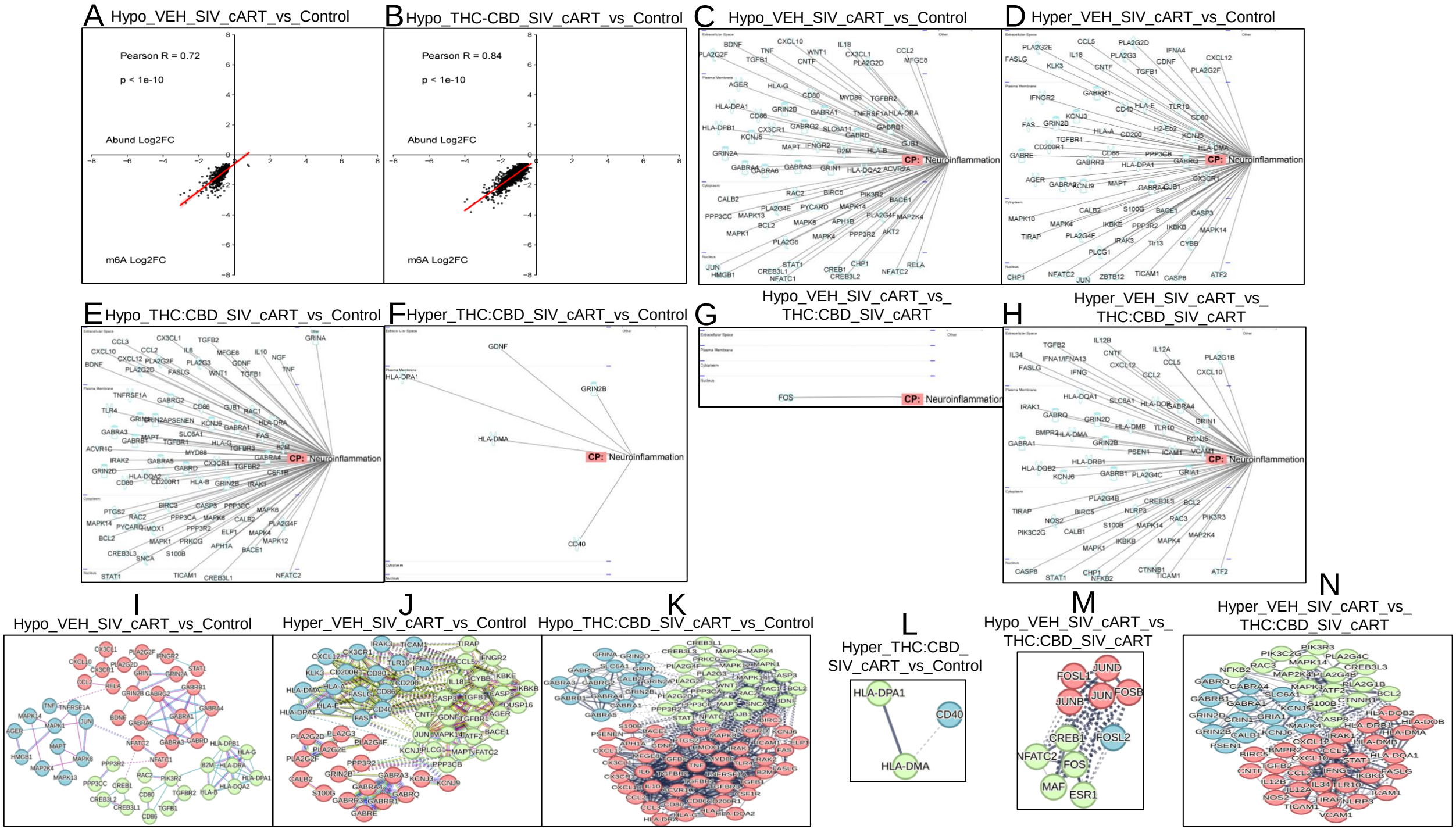
A
Hypo_VEH_SIV_cART_vs_Control
Pearson R = 0.72
p < 1e-10
Abund Log2FC
m6A Log2FC
B
Hypo_THC-CBD_SIV_cART_vs_Control
Pearson R = 0.84
p < 1e-10
Abund Log2FC
m6A Log2FC
C
Hypo_VEH_SIV_cART_vs_Control
CP: Neuroinflammation
D
Hyper_VEH_SIV_cART_vs_Control
CP: Neuroinflammation
E
Hypo_THC:CBD_SIV_cART_vs_Control
CP: Neuroinflammation
F
Hyper_THC:CBD_SIV_cART_vs_Control
GDNF
HLA-DPA1
GRIN2B
HLA-DMA
CD40
CP: Neuroinflammation
G
Hypo_VEH_SIV_cART_vs_
THC:CBD_SIV_cART
FOS
CP: Neuroinflammation
H
Hyper_VEH_SIV_cART_vs_
THC:CBD_SIV_cART
CP: Neuroinflammation
I
Hypo_VEH_SIV_cART_vs_Control
J
Hyper_VEH_SIV_cART_vs_Control
K
Hypo_THC:CBD_SIV_cART_vs_Control
L
Hyper_THC:CBD_
SIV_cART_vs_Control
HLA-DPA1
CD40
HLA-DMA
M
Hypo_VEH_SIV_cART_vs_
THC:CBD_SIV_cART
FOSL1
JUND
JUNB
JUN
FOSB
CREB1
FOSL2
NFATC2
FOS
MAF
ESR1
N
Hyper_VEH_SIV_cART_vs_
THC:CBD_SIV_cART

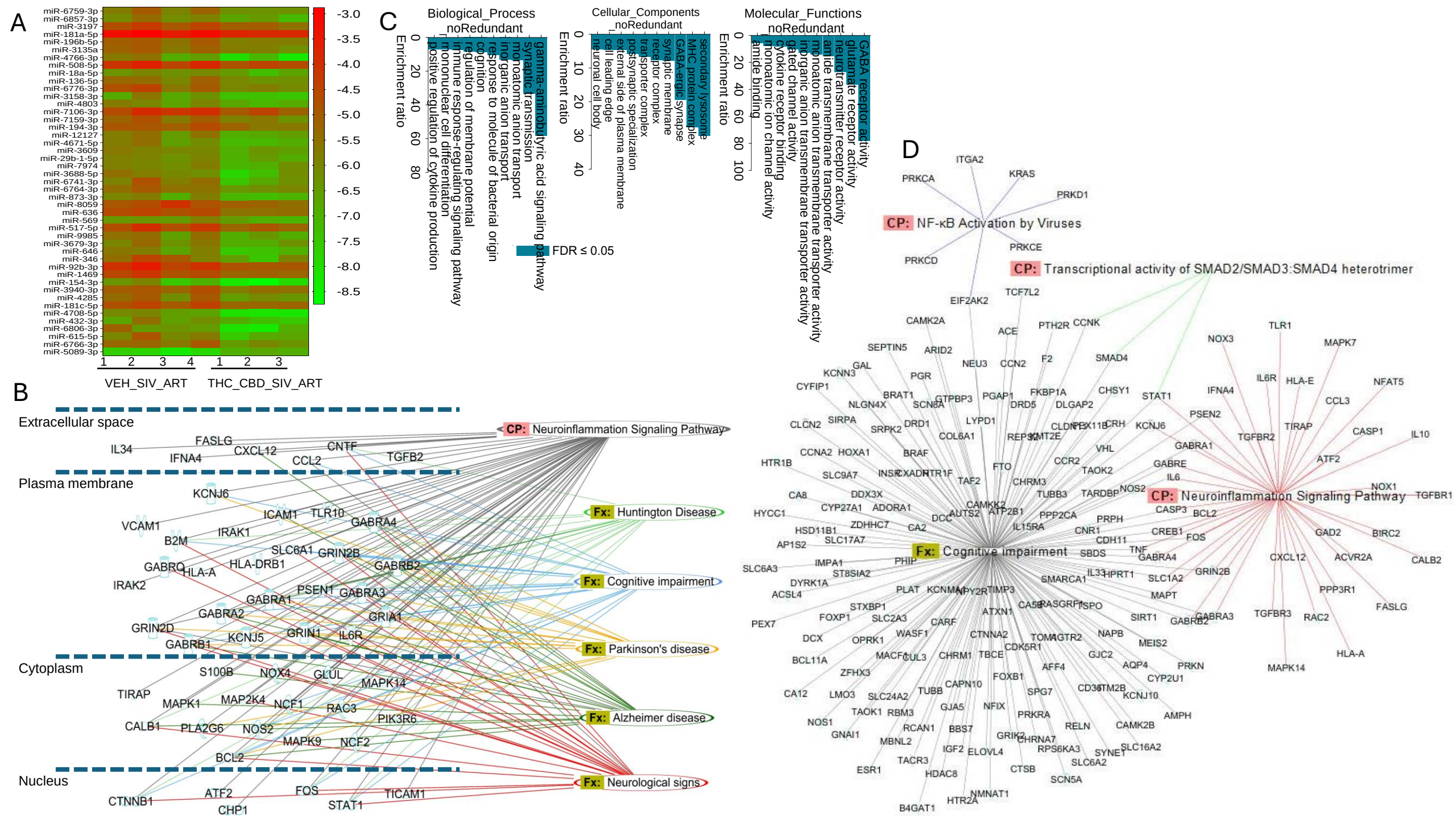
A
miR-6759-3p
miR-6857-3p
miR-3197
miR-181a-5p
miR-196b-5p
miR-3135a
miR-4766-3p
miR-508-5p
miR-18a-5p
miR-136-5p
miR-6776-3p
miR-3158-3p
miR-4803
miR-7106-3p
miR-7159-3p
miR-194-3p
miR-12127
miR-4671-5p
miR-369
miR-29b-1-5p
miR-7974
miR-3688-5p
miR-6741-3p
miR-6764-3p
miR-873-3p
miR-8059
miR-636
miR-569
miR-517-5p
miR-9985
miR-3679-3p
miR-646
miR-346
miR-92b-3p
miR-1469
miR-154-3p
miR-3940-3p
miR-4285
miR-181c-5p
miR-4708-5p
miR-432-3p
miR-6806-3p
miR-615-5p
miR-6766-3p
miR-5089-3p
-3.0
-3.5
-4.0
-4.5
-5.0
-5.5
-6.0
-6.5
-7.0
-7.5
-8.0
-8.5
1 2 3 4 1 2 3
VEH_SIV_ART
THC_CBD_SIV_ART
C
Biological_Process _noRedundant
gamma-aminobutyric acid signaling pathway
synaptic transmission
monoatomic anion transport
inorganic anion transport
response to molecule of bacterial origin
cognition
regulation of membrane potential
immune response-regulating signaling pathway
mononuclear cell differentiation
positive regulation of cytokine production
Enrichment ratio
0 20 40 60 80
Cellular_Components _noRedundant
secondary lysosome
MHC protein complex
GABA-ergic synapse
synaptic membrane
receptor complex
transporter complex
postsynaptic specialization
external side of plasma membrane
cell leading edge
neuronal cell body
Enrichment ratio
0 10 20 30 40
Molecular_Functions _noRedundant
GABA receptor activity
glutamate receptor activity
neurotransmitter receptor activity
amide transmembrane transporter activity
monoatomic anion transmembrane transporter activity
inorganic anion transmembrane transporter activity
gated channel activity
cytokine receptor binding
monoatomic ion channel activity
amide binding
Enrichment ratio
0 20 40 60 80 100
FDR ≤ 0.05
B
Extracellular space
Plasma membrane
Cytoplasm
Nucleus
CP: Neuroinflammation Signaling Pathway
Fx: Huntington Disease
Fx: Cognitive impairment
Fx: Parkinson's disease
Fx: Alzheimer disease
Fx: Neurological signs
IL34
FASLG
IFNA4
CXCL12
CCL2
CNTF
TGFB2
KCNJ6
VCAM1
ICAM1
TLR10
GABRA4
B2M
IRAK1
SLC6A1
GRIN2B
GABRQ
HLA-A
HLA-DRB1
GABRB2
IRAK2
PSEN1
GABRA3
GABRA1
GABRA2
GRIA1
GRIN2D
KCNJ5
GRIN1
IL6R
GABRB1
S100B
NOX4
GLUL
MAPK14
TIRAP
MAPK1
MAP2K4
NCF1
RAC3
PIK3R6
CALB1
PLA2G6
NOS2
MAPK9
NCF2
BCL2
CTNNB1
ATF2
FOS
TICAM1
CHP1
STAT1
D
CP: NF-κB Activation by Viruses
CP: Transcriptional activity of SMAD2/SMAD3:SMAD4 heterotrimer
CP: Neuroinflammation Signaling Pathway
Fx: Cognitive impairment
ITGA2
PRKCA
KRAS
PRKD1
PRKCE
PRKCD
EIF2AK2
TCF7L2
CAMK2A
ACE
PTH2R
CCNK
SEPTIN5
ARID2
NEU3
CCN2
F2
SMAD4
GAL
KCNN3
PGR
CYFIP1
BRAT1
GTPBP3
PGAP1
FKBP1A
CHSY1
STAT1
NLGN4X
SCN8A
DRD5
DLGAP2
CLCN2
SIRPA
SRPK2
DRD1
LYPD1
COL6A1
CRH
KCNJ6
CCNA2
HOXA1
BRAF
VHL
HTR1B
SLC9A7
CCR2
TAOK2
GABRE
IL6
TAF2
FTO
CHRM3
CA8
DDX3X
TUBB3
TARDBP
NOS2
HYCC1
CYP27A1
ADORA1
CAMKK2
ATP2B1
PPP2CA
PRPH
CASP3
BCL2
HSD11B1
ZDHHC7
CA2
IL15RA
CNR1
CREB1
FOS
AP1S2
SLC17A7
CDH11
SBDS
TNF
GABRA4
SLC6A3
IMPA1
PHIP
ST8SIA2
IL33
HPRT1
SLC1A2
GRIN2B
DYRK1A
SMARCA1
ACSL4
PLAT
TIMP3
MAPT
STXBP1
ATXN1
PEX7
FOXP1
SLC2A3
CARF
SIRT1
GABRB2
GABRA3
DCX
OPRK1
WASF1
CTNNA2
NAPB
MEIS2
BCL11A
CUL3
CHRM1
TBCE
CDK5R1
GJC2
AQP4
PRKN
ZFHX3
AFF4
CYP2U1
CA12
LMO3
SLC24A2
TUBB
CAPN10
FOXB1
SPG7
KCNJ10
TAOK1
RBM3
GJA5
NFIX
PRKRA
AMPH
NOS1
RCAN1
BBS7
RELN
CAMK2B
GNAI1
MBNL2
GRIK2
CHRNA7
IGF2
ELOVL4
RPS6KA3
SYNE1
SLC16A2
TACR3
SLC6A2
ESR1
HDAC8
CTSB
SCN5A
NMNAT1
HTR2A
B4GAT1
TLR1
NOX3
MAPK7
IL6R
HLA-E
NFAT5
IFNA4
CCL3
PSEN2
TIRAP
CASP1
IL10
TGFBR2
GABRA1
ATF2
NOX1
TGFBR1
GAD2
BIRC2
CXCL12
ACVR2A
CALB2
PPP3R1
FASLG
TGFBR3
RAC2
HLA-A
MAPK14

A

Human STAT1 ENST00000540176.1 3' UTR length: 3294

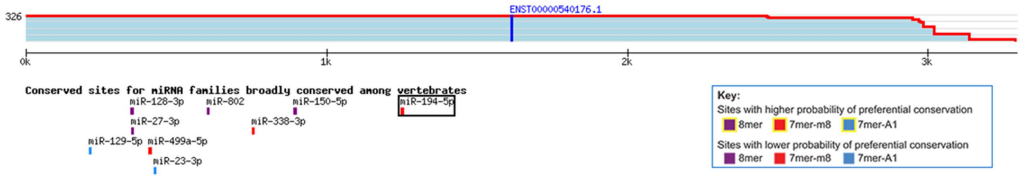

Conserved

	Predicted consequential pairing of target region (top) and miRNA (bottom)	Site type	Context++ score	Context++ score percentile	Weighted context++ score	Conserved branch length	P_{CT}	Predicted relative K_D
Position 1248-1254 of STAT1 3' UTR hsa-miR-194-5p	5' ...AGAAAGAACUUUCUGCUGUUACU... 3' AGGUGUACCUCAACGACAAUGU	7mer-m8	-0.11	78	-0.11	3.799	N/A	-5.053

B

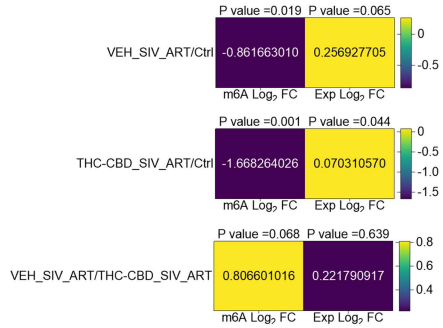

C

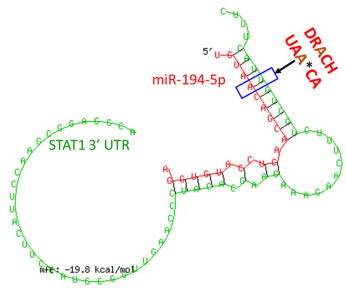

miR-194-5p- STAT1 pairing

miR-194-5p- UGUUAA*CAGCAACUCCAUGUGGA (STAT1)

Negative control | Wild Type | M6A modified

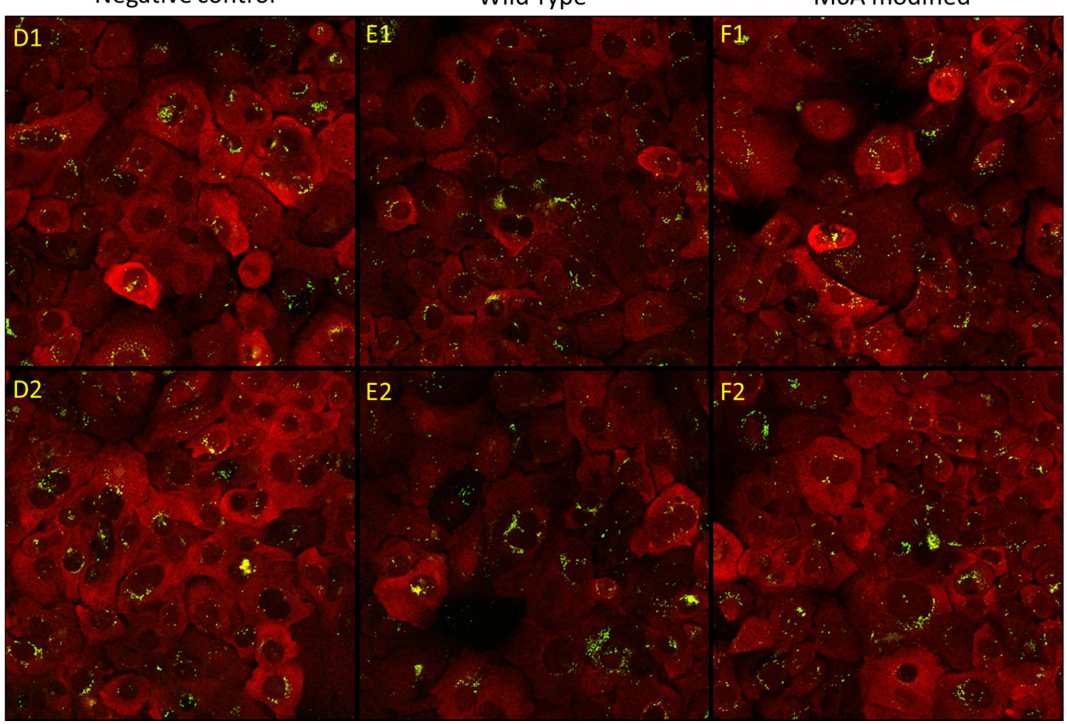

G

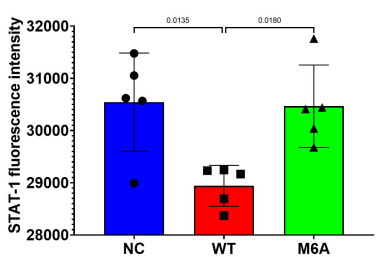

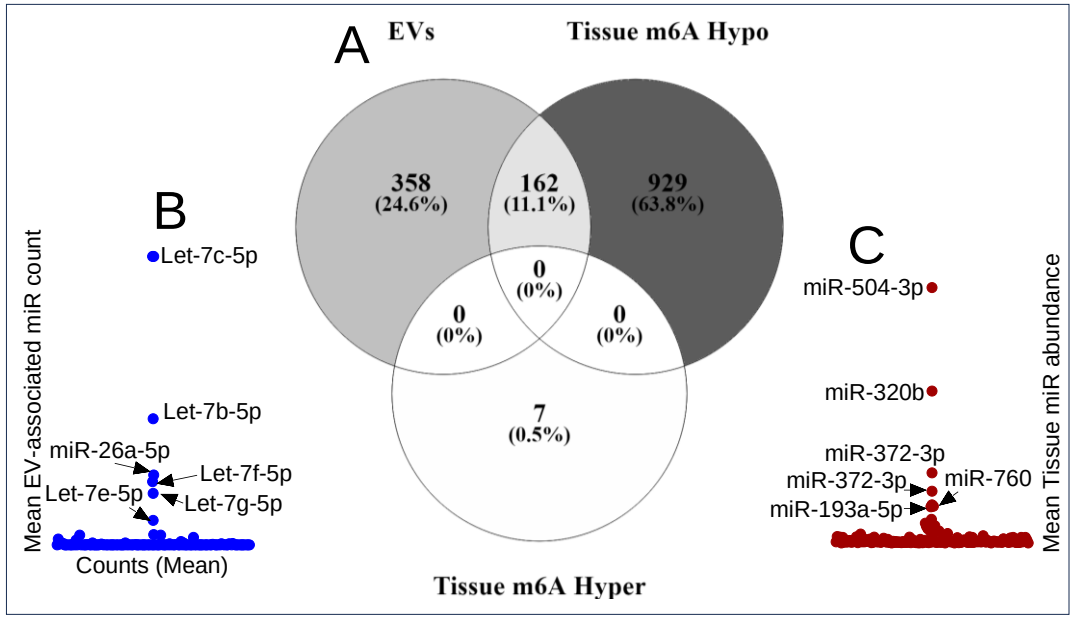
A
EVs
Tissue m6A Hypo
358
(24.6%)
162
(11.1%)
929
(63.8%)
0
(0%)
0
(0%)
0
(0%)
7
(0.5%)
Tissue m6A Hyper
B
Let-7c-5p
Let-7b-5p
miR-26a-5p
Let-7f-5p
Let-7e-5p
Let-7g-5p
Mean EV-associated miR count
Counts (Mean)
C
miR-504-3p
miR-320b
miR-372-3p
miR-372-3p
miR-760
miR-193a-5p
Mean Tissue miR abundance

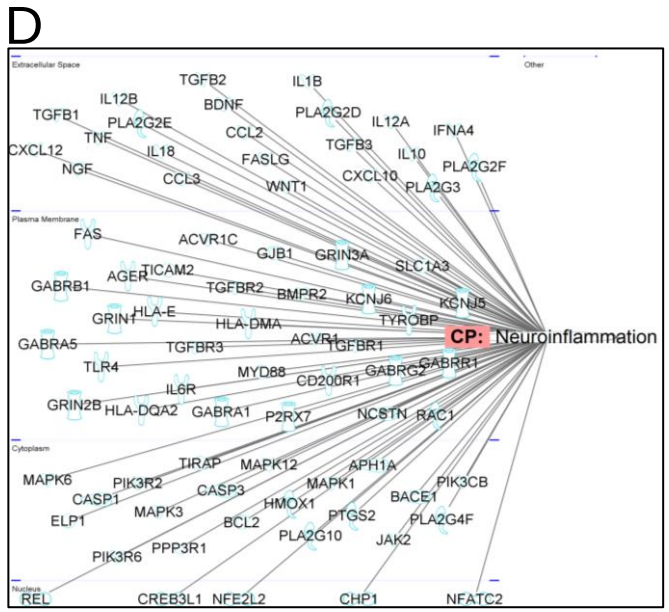
D
CP: Neuroinflammation

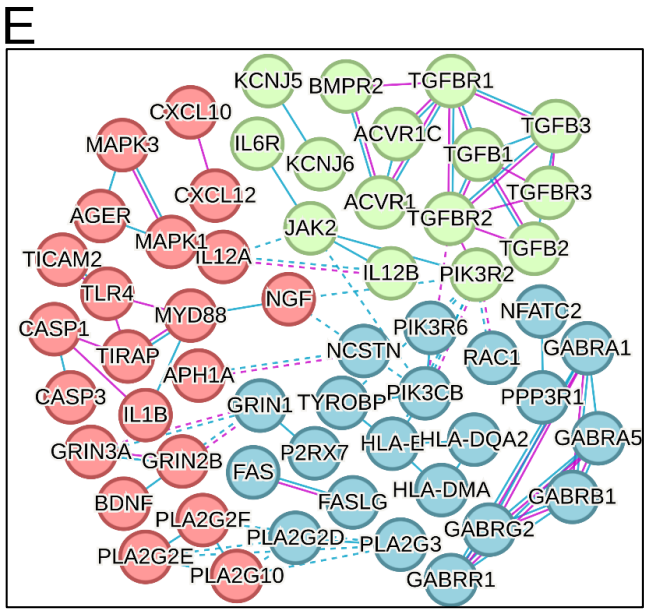
E

F
5 10 15 20
-Log10 of FDR
positive regulation of response to external stimulus
neuron death
regulation of leukocyte activation
positive regulation of cell motility
T cell activation
regulation of cell-cell adhesion
positive regulation of cell activation
log2 of enrichment ratio